Title

GRIP-tape: A Novel Design of Tape-Based Manipulator

Author

He, Gengzhi

Publication Date

2023

Peer reviewed|Thesis/dissertation

UNIVERSITY OF CALIFORNIA SAN DIEGO

GRIP-tape: A Novel Design of Tape-Based Manipulator

A Thesis submitted in partial satisfaction of the requirements
for the degree Master of Science

in

Engineering Sciences (Mechanical Engineering)

by

Gengzhi He

Committee in charge:

Professor Nicholas Gravish, Chair
Professor Shengqiang Cai
Professor Michael Yip

2023

The Thesis of Gengzhi He is approved, and it is acceptable in quality and form for publication on microfilm and electronically.

University of California San Diego

2023

TABLE OF CONTENTS

LIST OF FIGURES

LIST OF ABBREVIATIONS

GRIP-tape	Grasping and Rolling In Plane - tape
DOF	Degrees of freedom

VITA

2020 Bachelor of Engineering in Mechanical Engineering, Wuhan University of Technology

2023 Master of Science in Engineering Sciences (Mechanical Engineering), University of California San Diego

FIELD OF STUDY

Major Field: Robotics

Studies in Soft Robotics

Professor Nicholas Gravish

ABSTRACT OF THE THESIS

GRIP-tape: A Novel Design of Tape-Based Manipulator

by

Gengzhi He

Master of Science in Engineering Sciences (Mechanical Engineering)

University of California San Diego, 2023

Professor Nicholas Gravish, Chair

The GRIP-tape project aims to develop structures and mechanisms that utilize appendages constructed from tape springs, serving as gripper fingers. The inherent stiffness of the unbent segment of the tape spring provides the necessary support for gripping forces, while the flexible, bent part (i.e., the fingertip) can be smoothly moved along the tape by altering the shape of the triangular appendage. Additionally, the springy tip permits a gentle pinch without causing damage.

To achieve precise control for the appendage, I have constructed both forward and inverse kinematics. These models facilitate the accurate positioning and control of the fingertip through the use of seven motors at the base. By initially determining the length of the already extended tape, I can locate the fingertip in a two-dimensional plane. The inverse kinematics model specifies the necessary extension or retraction of each side of the appendage to move the fingertip to a desired location. Furthermore, it can predict the fingertip's location using forward kinematics and data collected from DYNAMIXEL motors.

The key features of GRIP-tape include object gripping, translation in two modes, and rotation, making it a versatile and adaptable system for various applications. Additionally, by incorporating a load cell as the sensor at the base, we've expanded the utility of GRIP-tape to include automated tasks such as searching and measurement.

INTRODUCTION

A wide array of robotic grippers has been created for use as end effectors for robot manipulation. When coupled with robotic arms, they are typically employed for the rotation and translation of target objects where the gripper holds the object, and the robot arm provides the translation and rotation.

Certain grippers have also integrated active surfaces, enabling them to perform various forms of in-hand manipulation. Like the underactuated modular finger featuring a pull-in mechanism [1], aimed at streamlining actuation. Velvet Fingers [2], prioritizing the stability of grasp, and the Sheet-Based Gripper [3], concentrating on refining the object-picking process. These advancements leverage the dynamic surfaces on the fingers to enable complex in-hand maneuvers such as twisting and pulling, thereby enhancing the overall stability during gripping actions. However, the need for rollers within the fingers or the finger's supportive skeletal structure for the “conveyor belt” constrains the choice of rigid materials for constructing the fingers, thereby restricting their flexibility. The absence of feedback could potentially result in an issue where delicate items might experience harm during the gripping process.

For long-range extension, different methods and structures have been developed, mostly soft robots. Some are built by inflatable membranes such as growing soft robots guided by control chambers [4], electromagnetic [5], and predefined patterns [6]. Some utilize the unfolding of origami-inspired design to accomplish extension [7][8]. The limit of most of these kinds of designs is stiffness, without a self-locking mechanism, the external load of these robotic arms is not easy to predict and control, especially for soft robots.

Another method of extension that has been discovered is using a tape spring-like structure. The softness of the tape spring enables it to be rolled up into a small container. After it gets extended, the curvature on the tape spring provides a certain amount of durability against the external moment, at this point, the tape spring can be seen as a rigid beam. Many publications like the extension nail mechanism built by Junya Tanaka et al [9] and tape-spring manipulators built by Yi Yang et al [10] have shown the stiffness of tape springs pushing against an object along its outward radial direction and holding it against gravity. The Robotic limbs using tape springs by Justin Quan et al [11] and The Amoeba-inspired swimming robot by Curtis Spark et al [12] utilized the force durability of tape springs along its tangential direction and continuous shape change of tape springs with a bending.

In this thesis, I present the design of a gripper that draws inspiration from several key attributes of tape springs, as illustrated in Figure I.1a. The incorporation of these characteristics has significant implications for the functionality of the gripper. Firstly, the softness inherent to tape springs ensures the extensibility of the gripper fingers and imparts a springy touch at the tips of the appendage, enhancing its ability to interact with objects delicately. Secondly, the stiffness of the thin shell structure that resists bending exhibited by the extended tape springs plays a pivotal role in the gripper's performance as the stiffness enables the gripper to bear the gripping force, thereby ensuring its capability to grasp and manipulate objects effectively. The capacity for smooth reconfiguration allows it to move with ease across a 2-D plane. By harnessing these characteristics of tape springs, our gripper design exhibits a unique combination of extensibility and stiffness, making it a promising solution for applications requiring dexterous manipulation, and the ability to handle objects from a longer distance.

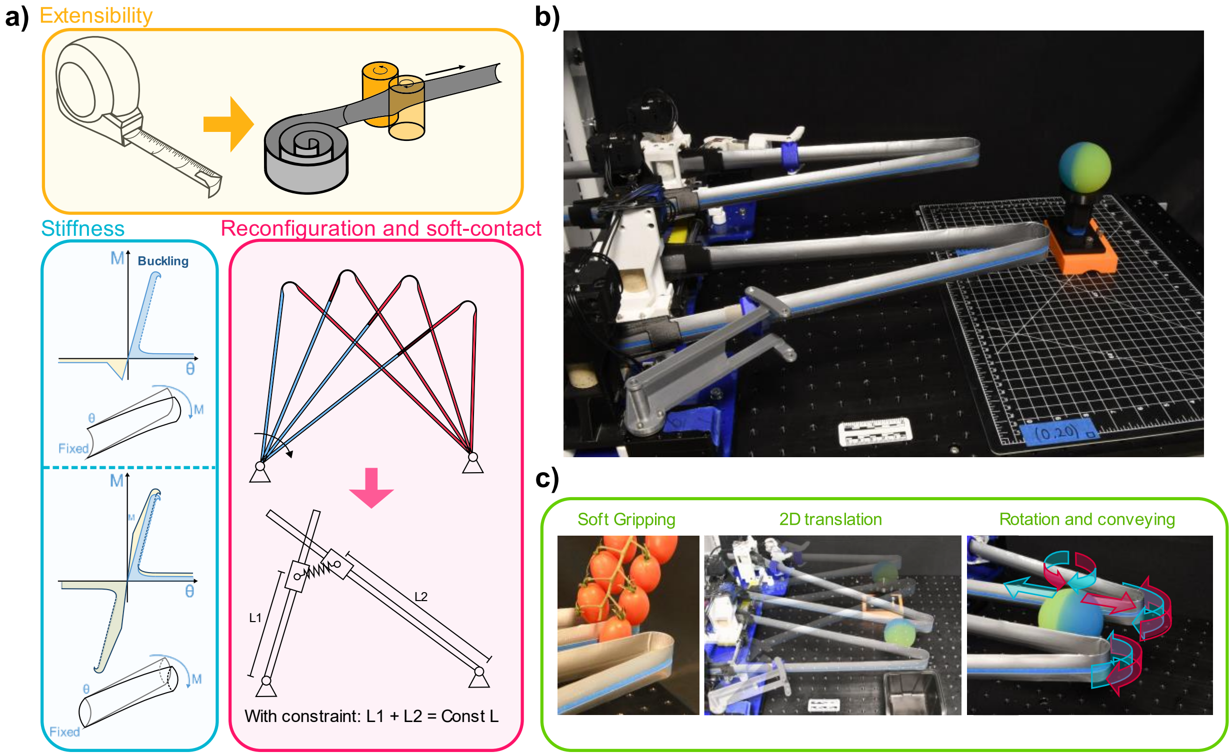

Figure I.1.1: Introduction

1.1 Buckling Force

Before designing the mechanism, I first analyzed the mechanical performance of extended tape springs to validate that enough gripping force could be supported by extended tape springs.

1.1.1 Bidirectional tape

Since the tape spring is only stiff when force applied on one side of it, to make the deployable tape capable to supply force on both sides, we designed a configuration called Bidirectional tape which is made of two pieces of tape springs stacked in a counter direction and bounded with duct tapes (Figure 1.1),

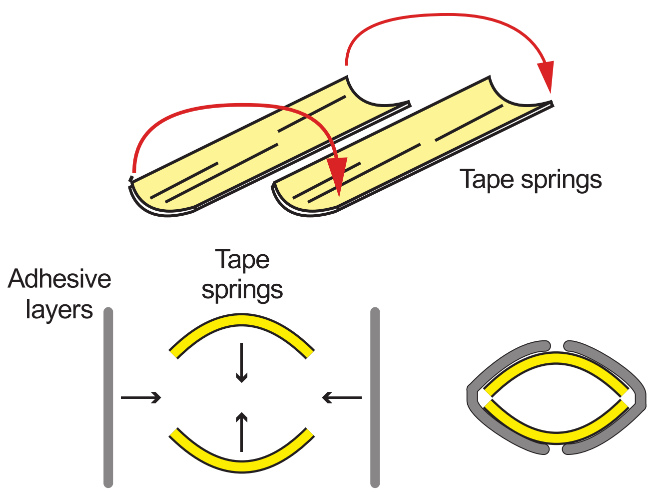

Figure 1.1: Bidirectional tape [13].

1.1.2 3-point bend tests

I conducted a 3-point bending test. The results, as depicted in Figure 1.2, reveal that the bidirectional tape exhibits the highest buckling force, indicated by the load peak. Conversely, in the case of the unidirectional tape loaded on the concave side, there is no clear drop in the load-displacement curve, implying the absence of buckling in this instance. Due to the geometric relationship inherent in bidirectional tapes, the displacement can be viewed as the combined effect of two unidirectional tapes reacting to the same applied load. Theoretically, the rate of load increase concerning displacement for the bidirectional tape should be slightly greater than the average of the rates of increase for the two unidirectional tapes. This is because the elasticity of the duct tape also contributes to resisting the applied load. It's important to note that in tests involving the unidirectional tape loaded on both the convex and concave sides, friction between the platform and the two edges of the tape hinders deformation, resulting in an increase in the recorded load.

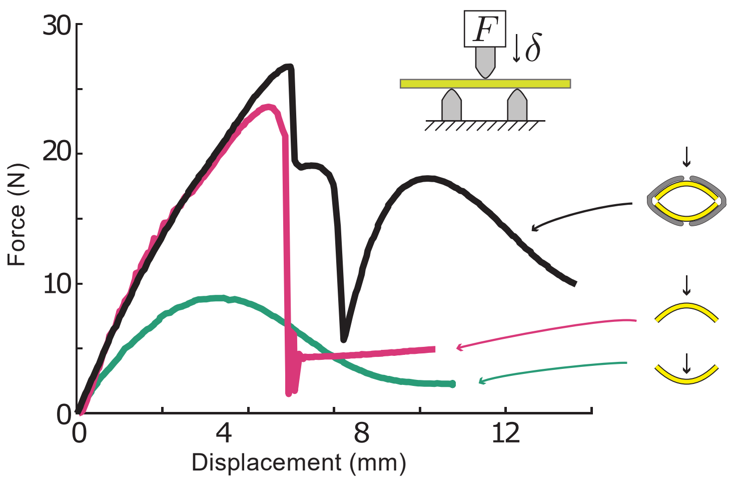

Figure 1.2: Result of 3-point bend test.

1.1.3 Rotation bend test

With 1 side of the tape spring fixed on a rotation stage, the other side is free and desired to hit and press on a load cell (Figure 1.3). The load cell reads the maximum force that tape springs can handle before buckling. I did the test on 3 different configurations of tape springs: Unidirectional tape (a normal tape spring pushed from its stronger side), Bidirectional tape, and Double-stacked (two pieces of tape springs stacked in the same direction). For the last one, I have two sets of data gained from two directions of the load.

Figure 1.4 is a plot showing 1 of the trials of force reading as rotating the base back and forth. During the rotation of the stage, a consistent force increase is observed until the angle reaches approximately 6 degrees, identified as the buckling angle, correlating to a buckling force of about 5N. After this angle is reached, the rotation stage reverses direction based on a predefined angle.

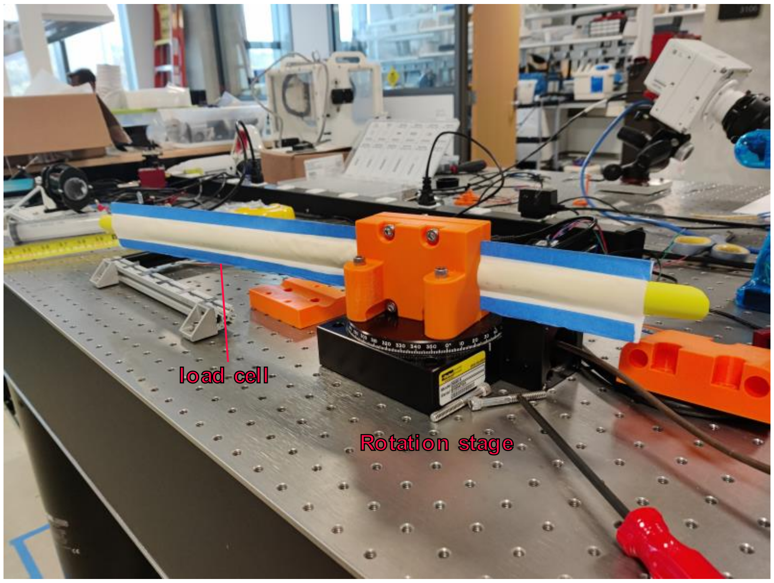

Figure 1.3: Bend test on rotation stage.

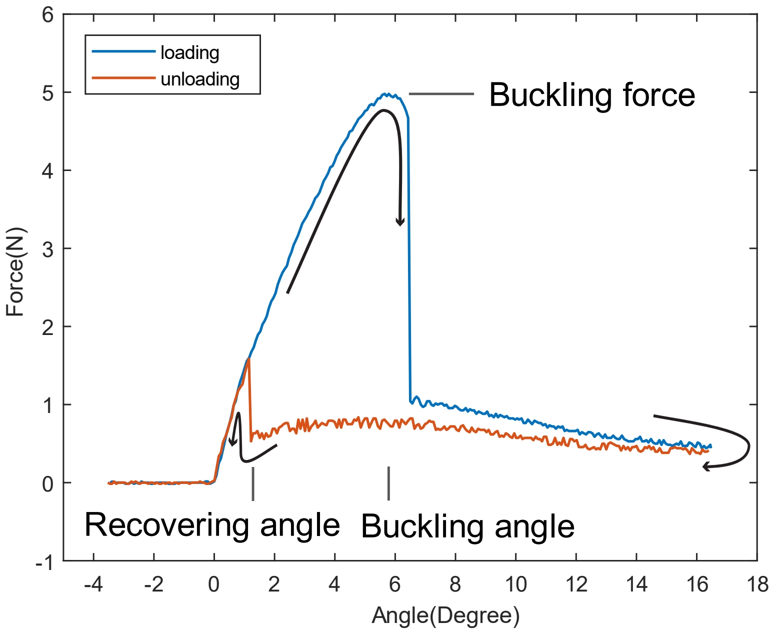

Figure 1.4: 1 trial of bend test on rotation stage.

The tape exhibits its self-recoverability after reaching a specific angle, referred to as the recovering angle. Notably, this recovering angle tends to be smaller than the initial buckling angle. Consequently, the tape's recovery necessitates returning to a position preceding the angle where it originally buckled.

Test on different tapes at different distances L, as shown in Figure 1.5. We know the buckling moment of an extended tape spring is approximately a constant value, thus the force and length of the tape can be fitted to an inversely proportional relationship with some offset. the buckling force of the double-stacked tape is almost double the bucking force of the unidirectional tape. However, the performance of the bidirectional tape is better than half of the add-up of the two double-stacked configurations. One possible reason could be the balance of two tapes placed in the counter direction increased the stability of the beam under loading force.

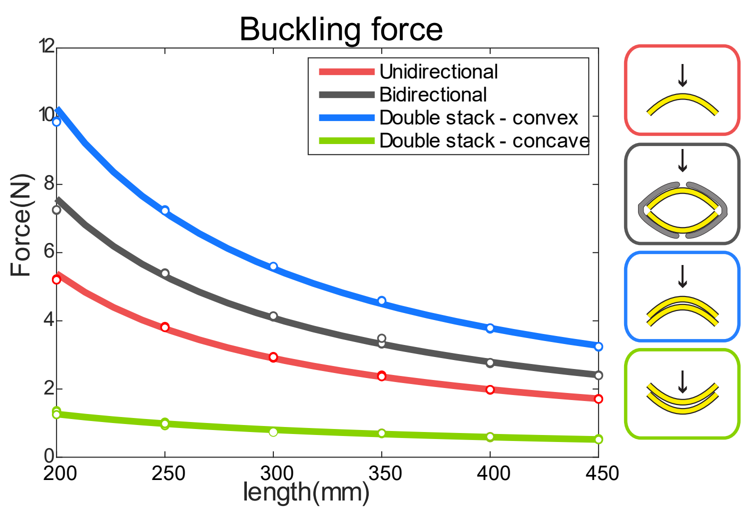

Figure 1.5: Comparison of the results for different tapes.

1.1.4 Fatigue test

An important feature of the tape appendages is, unlike other rigid materials, tape spring is self-recoverable after buckling once there is enough space for it to recover. Hence, I did a fatigue test to see if the mechanical property of the tape spring would be largely affected by thousands of times of buckling. Similar to the setup of the previous test, I mounted a load cell on a track 20 cm away from the starting point of the tape spring and used a rotation base to rotate the tape spring to a certain angle. During the rotation, the tape measure contacts the load cell, buckles, stops at a certain angle, and rotates back to the initial angle. I gathered the data of 4000 cycles from the load cell including at which angles the tape spring buckles (Figure 1.7a) and recovers (Figure 1.7c), and what are the maximum forces before buckling (Figure 1.7b). After 4000 trials, the bucking angle didn't change significantly, the bucking force reduced from 4.97N to 4.915N, and the recovering angle reduced from 1.28 degrees to 1.16 degrees. In the scale of the current design, such an amount of digression is acceptable.

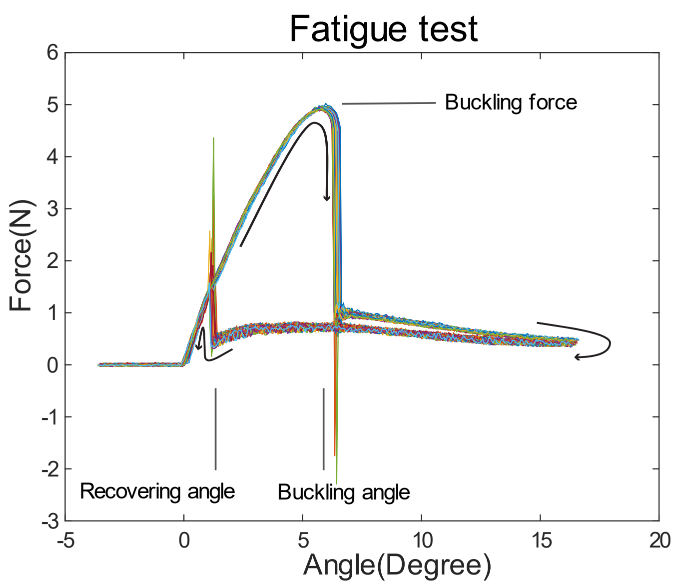

Figure 1.6: Fatigue test.

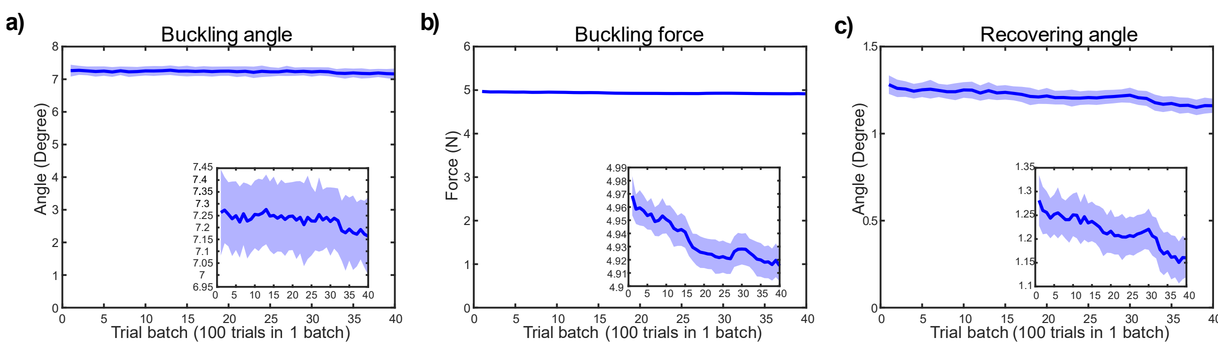

Figure 1.7: Trending of the fatigue test.

1.2 Stiffness of the tip

The structure of one appendage of GRIP-tape can be simplified as two links connected by a nonlinear spring on the tip of the appendage, while the perimeter of this triangular shape is constant. Since the change in the length of each link only involves a small amount of energy gain or loss, the transformation is quite fluent. And since the tip of the appendages are bent, its comparatively soft. After I did some experiments on the bending section and curve fitting, the stiffness of the spring-like bending can be represented in Figure 1.8 as:

$$\text{Bidirectional: } F = 0.00358 * x^3 + 0.00341 * x^2 + 0.66343 * x$$

$$\text{Unidirectional}_{\text{convex}}\text{: } F = 0.00144 * x^3 + 0.00266 * x^2 + 0.21346 * x$$

$$\text{Unidirectional}_{\text{concave}}\text{: } F = 0.00138 * x^3 + 0.00269 * x^2 + 0.20614 * x$$

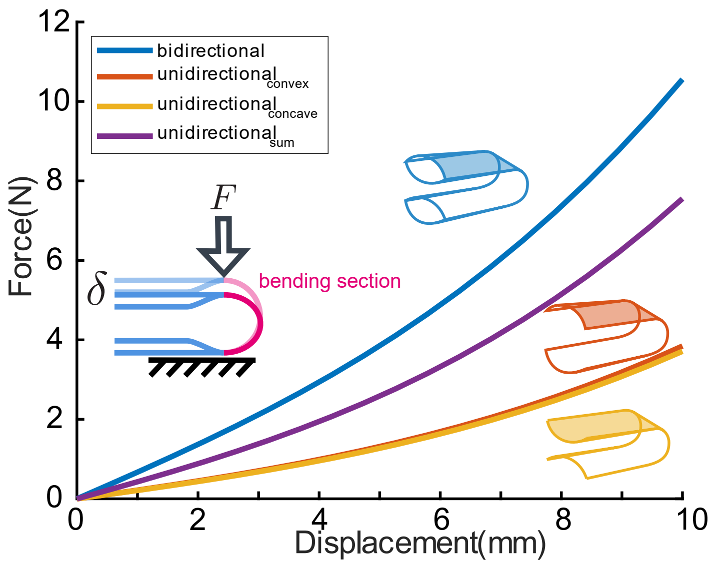

Figure 1.8: Comparison on stiffness of the tip.

The non-linearity in the relationship means a higher load leads to higher spring stiffness. The results for the two unidirectional tapes are similar, for the bidirectional tape, the total load exceeded the sum of the loads of the unidirectional tapes under the same displacement. This discrepancy may arise from friction between the two pieces of tape and the stretching stiffness of the duct tape. It is worth mentioning that due to the properties of duct tape, the loading stiffness curve and unloading stiffness curve did not perfectly overlap, as shown in Figure 1.9.

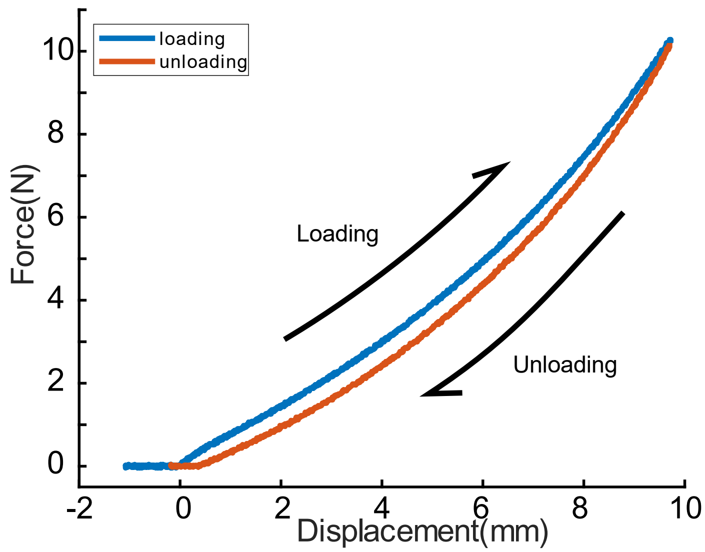

Figure 1.9: Load and unload cycle.

When likening the bending area to a $15mm * 25.4mm * 30mm$ cube and calculate its strain stress curve (Figure 1.10), the Young's modulus of it compared with other soft materials in Figure 1.11, it indicates that the performance is close to silicone elastomer. The springy performance introduces some degrees of softness that allows gentle gripping on delicate objects. Figure 1.12 depicts an escalating curvature corresponding to increased gripping force, a departure from the rigid structure of conventional gripper fingers. The flexible nature of the springy tip of the appendage offers a visible representation of force input and allows for a larger tolerance of angular displacement without damaging the object.

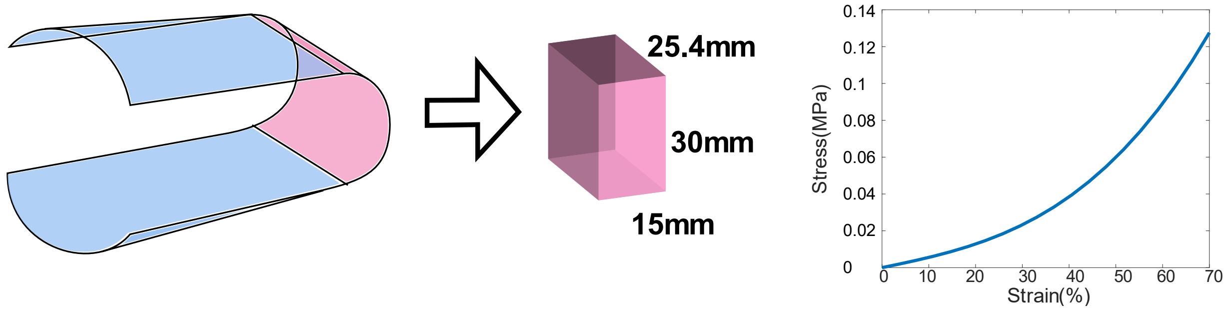

Figure 1.10: Strain stress curve.

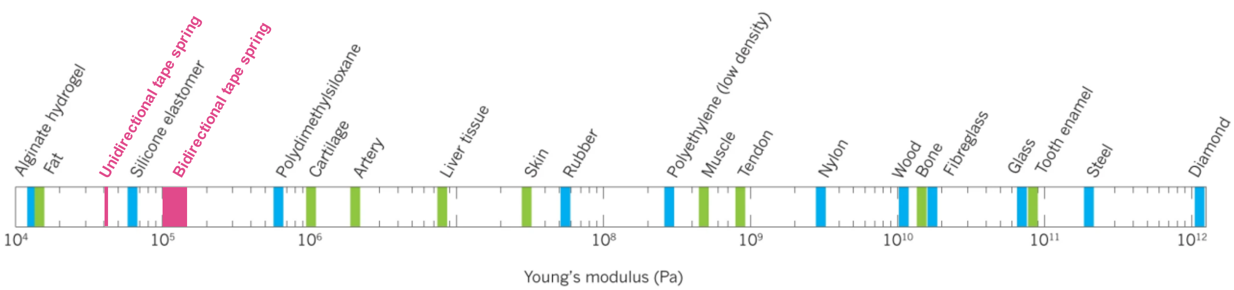

Figure 1.11: Young's modulus comparison with other materials. (Adapted from [14])

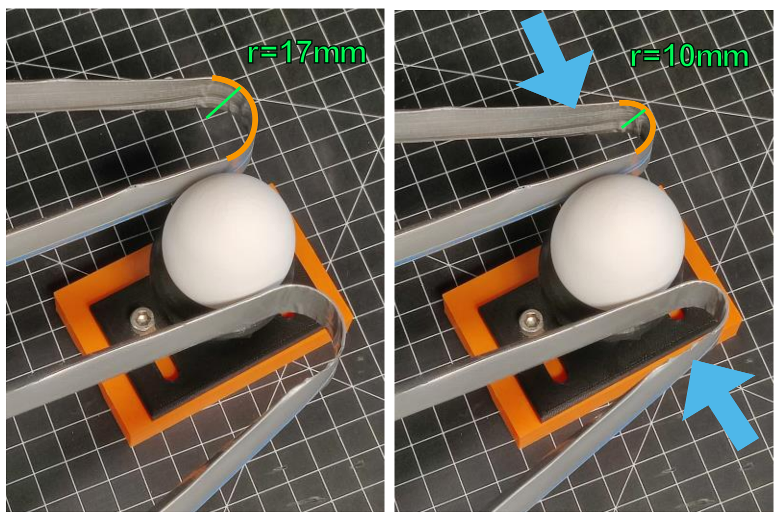

Figure 1.12: Soft grip.

Chapter 2 GRIP-tape: modeling and design

2.1 Modeling

2.1.1 Inverse kinematics

Another main utility of tape springs in the design is based on their ability to transfer the buckling point along the body while keeping the perimeter constant. This buckling point transportation can be seen as changing the length of the two links while keeping the sum of the lengths constant. Based on this feature, some functions like rotation can be achieved by keeping the sum of the length of each side of the appendage constant while changing the length individually at an equal speed but in different directions. Furthermore, since we are controlling the extruding and retracting length of both sides of the appendage which is the overall length of the appendage rather than controlling the length of the two links directly, to make the tip of the appendage reach a certain coordinate, the targeting overall length of the appendage can be reached by controlling the tape extruders on each side individually. Individual control of the two tape extruders will be discussed in Demonstration. 1 appendage of GRIP-tape has 3 degrees of freedom, 2 length control, and 1 angular control (θ_4), with the width control (length of a), the overall degrees of freedom of GRIP-tape is 7 (4 DOFs for length, 2 DOFs for angle, and 1 DOF for width).

To better define this model, the overall length of a appendage is no longer considered as one variable L which is separated into 3 sections as 3 variables. (i.e., the supporting section L_1, the interacting section L_2, and the bending section L_3) (Figure 2.1)

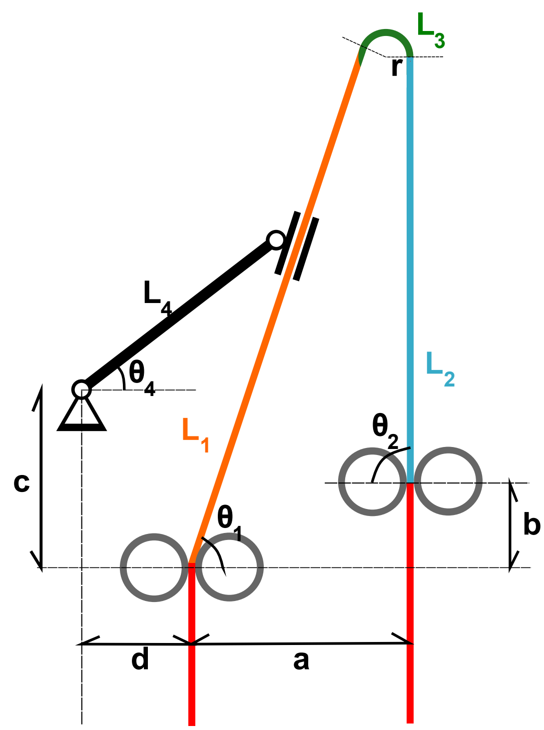

Figure 2.1: Modeling.

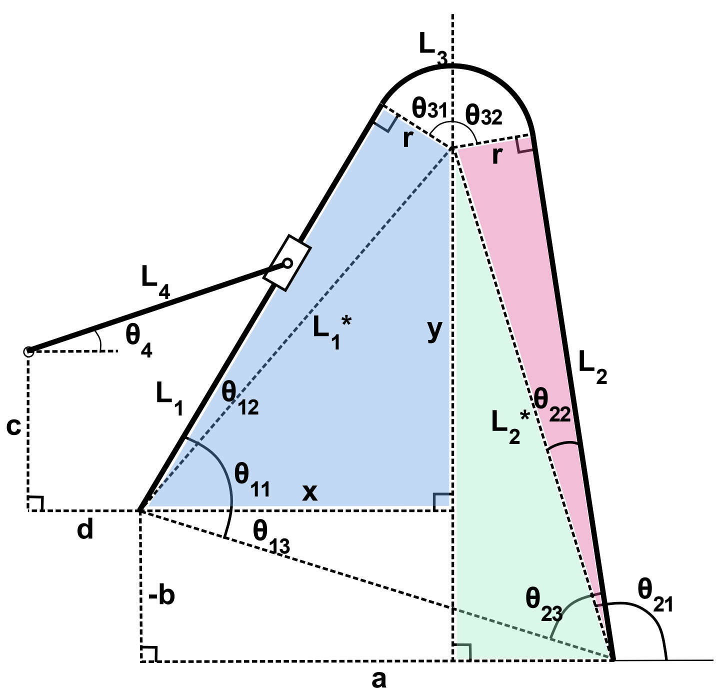

Figure 2.2: Inverse kinematics.

a, b, c, d, r, L_4, x, and y are given variables, using the inverse kinematics (Adapted from [12]) solve for L_1, L_2, L_3, and θ_4. Shown in Figure 2.2, the first step is finding the hypotenuses L_1^* and L_2^*. The former can be calculated as the square root of x square plus y square, similarly, the latter can be represented by the square root of $(x - a)$ square plus $(y - b)$ square. Knowing L_1^*, L_2^*, and r, the right triangles (marked in red) on both sides are fully defined. From it, comes the length of L_1^*, L_2^*, and angles θ_{12}, θ_{22}. The length of L_3 is defined as $(\theta_{31} + \theta_{32}) * r$. While $\theta_{31} = \theta_{11} + \theta_{12}$ because of the 2 right angles in the blue quadrangle, similarly $\theta_{32} = (\pi - \theta_{21}) + \theta_{22}$. θ_{11} and θ_{21} can be easily derived from another 2 right triangles (marked in green) as $\theta_{11} = arctan(y/x)$, $\theta_{21} = -arctan((y - b)/(a - x))$. Until now, the only unknown is θ_4. Solve $\theta_{11} + \theta_{21} = arctan((L_4 * \sin(\theta_4) + c)/(L_4 * cos(\theta_4) - d))$, θ_4 is found. An alternative solution of θ_4 is geometric calculations without involving any solvers.

IK In equations:

$$L_1^* = \sqrt{}(x^2 + y^2)$$

$$L_2^* = \sqrt{}((a - x)^2 + (y - b)^2)$$

$$\theta_{11} = tan^{-1}(y/x)$$

$$\theta_{21} = -tan^{-1}((y - b)/(a - x))$$

$$\theta_{12} = sin^{-1}(r/L_1^*)$$

$$\theta_{22} = sin^{-1}(r/L_2^*)$$

$$\theta_3 = \theta_{31} + \theta_{32} = \theta_{11} + \theta_{12} + (\pi - \theta_{21}) + \theta_{22}$$

$$L_1 = L_1^* * cos(\theta_{21})$$

$$L_2 = L_2^* * cos(\theta_{22})$$

$$L_3 = \theta_3 * r$$

$$\theta_{11} + \theta_{12} = \tan^{-1} \; ((L_4 * \; sin(\theta_4) + c)/(L_4 * \; cos(\theta_4) - d))$$

Alternative solution of θ_4:

$$\theta_c \; = \; arctan(c/d)$$

$$\theta_f \; = \pi \; - \theta_c \; - \theta_1$$

$$e \; = \sqrt{(d^2 + c^2)}$$

$$\theta_5 \; = \; arcsin(sin(\theta_f) * e/L_4)$$

$$\theta_4 \; = \theta_1 - \theta_5$$

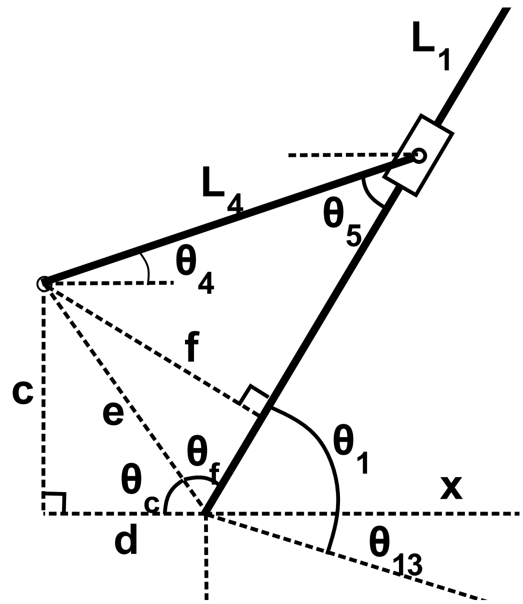

Figure 2.3: Alternative solution of θ_4

2.1.2 Forward kinematics

For the forward kinematics, it outputs the coordinate of the center of the arc given a, b, c, d, r, L_4, θ_4 and the total length L.

We used θ_4 to derive θ_1:

$$\theta_1 = \theta_{11} + \theta_{12} = atan((L_4 * sin(\theta_4) + c)/(L_4 * cos(\theta_4) - d))$$

L_1, L_2, and θ_2 can be derived by solving these equations:

$$L \; = \; (L_1 + L_2 + r * (\theta_1 - \theta_2 + \pi))$$

$$L_1 * sin(\theta_1) + r * sin(\theta_1 - \pi/2) \; = (L_2 * sin(\theta_2) + r * sin(\theta_2 + \pi/2) + b)$$

$$L_1 * cos(\theta_1) + r * cos(\theta_1 - \pi/2) \;=\; (L_2 * cos(\theta_2) + r * cos(\theta_2 + \pi/2) + a)$$

The coordinate of the center of the arc is:

$$x \;=\; L_1 * c\,os(\theta_1) + r * cos(\theta_1 - \pi/2)$$

$$y \;=\; L_1 * sin(\theta_1) + r * sin(\theta_1 - \pi/2)$$

2.2 Design and workspace

As depicted in Figure 2.4, the system is powered by a total of 7 motors. Four of these motors are dedicated to controlling the length of the tape springs. Additionally, two motors on each side are linked to angular control beams. The final motor is employed for adjusting the parameter a.

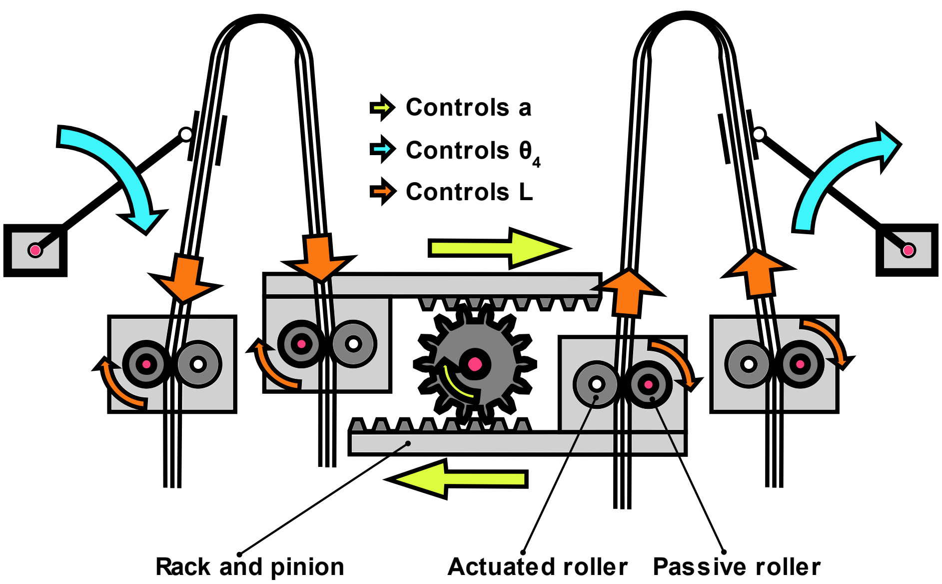

Figure 2.4: Schematics of the design.

The tape extruder comprises a case housing two rollers. One roller is motor-driven, while the other rotates freely. Each appendage is controlled by two extruders. In the context of controlling the appendage's length, both extruders contribute to determining the total length, denoted as L. Angular orientation of the appendage primarily relies on an angular control unit.

This unit features a guiding ring coated with low-friction material and an angular control beam powered by motors positioned on either side of the gripper. The beams pivot fixed perpendicularly to the base board, and the extruder close to the pivot is also fixed, resulting in predetermined and non-adjustable values for parameters c and d.

Parameter a's adjustability is designed to accommodate gripping and conveying objects of varying sizes. This adaptation is facilitated by a rack and pinion mechanism. Notably, orientation of the paralleled racks sets parameter b as a fixed and non-adjustable value.

The length of supporting section L_1, the interacting section L_2, and the bending section L_3 are determined automatically by the forward kinematics with input of L, a, and θ_4.

Concerning the system's workspace (Figure 2.5), the left boundary (marked with blue) is constrained by the tape coming into contact with the pivot of the angular control beam. The right boundary (marked with green) is limited by the angular control beam encountering the extruders. The inner boundary (marked with red) is defined by the length of the angular control beam, ensuring the guiding ring of the angular control unit doesn't interfere with the tape.

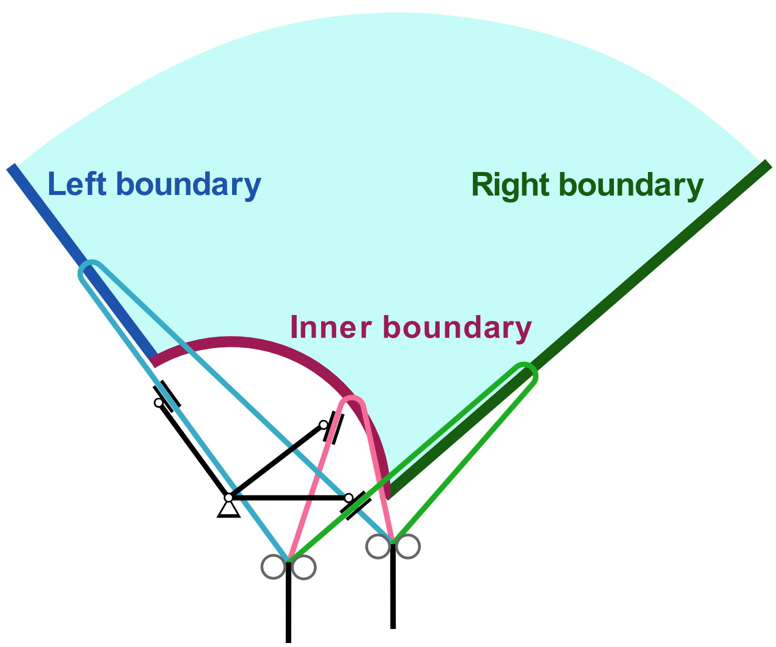

Figure 2.5: Work space.

Chapter 3 GRIP-tape: CAD and programming

3.1 CAD

3.1.1 Layout

The fabrication setup (Figure 3.1) mirrors the model discussed in the previous chapter. The layout includes 2 extruders positioned at the far left and far right of an acrylic base, directly controlling the outer section of the appendages. Additionally, 2 extruders are managed by a rack and pinion mechanism located on a track in the middle. The angular control beams is linked to motors fixed directly on the base. In this design, there are 7 DYNAMIXELs employed, consisting of 5 XL430-W250-T units with a maximum stall torque of 1.5 Nm, and 2 XM540-W270-T units capable of delivering a stall torque of 10.60 Nm. The latter are utilized in constructing the angular control units, where substantial torque is necessary.

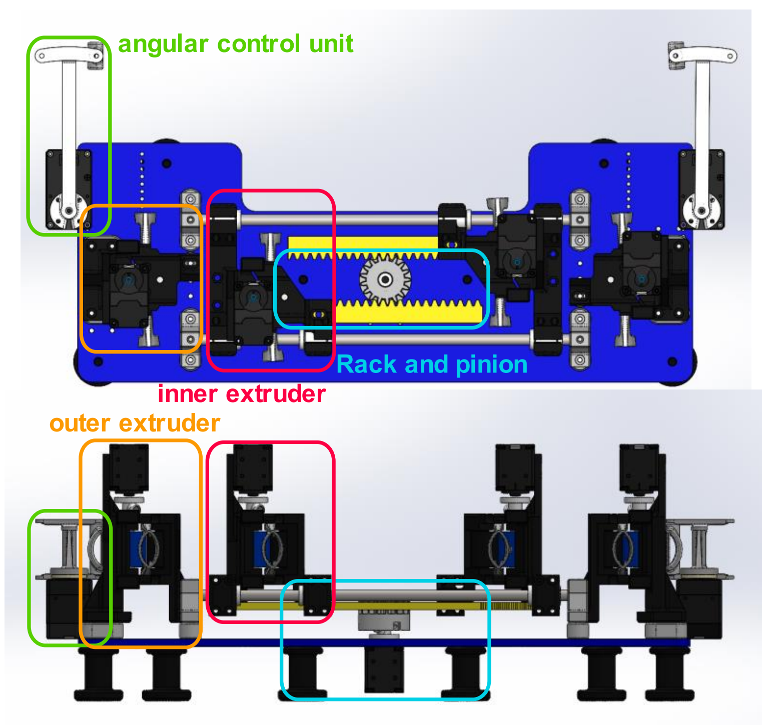

Figure 3.1: Layout.

3.1.2 Extruder

The extruder design, detailed in Figure 3.2, operates through a DYNAMIXEL XL430-W250-T motor, bifurcated into active and passive sections. Each segment features a roller on a shaft supported by 5mm*10mm*4mm bearings. The sections are encased together by four M3 screws, maintaining pressure on the rollers and facilitating friction adjustment as the screws' tightness regulates the roller-tape friction. The active roller is covered with sandpaper for increased traction. The extruder includes entrance and exit guides shaped to accommodate tape deformation to provide even support along the tape as they transform from soft to rigid. These guides play a crucial role in preventing the emerge of undesired bend caused by potential deformations in the tape due to its softness when compressed between the two rollers and subjected to external forces. Figure 3.3 provides a comparison between scenarios with and without guide support.

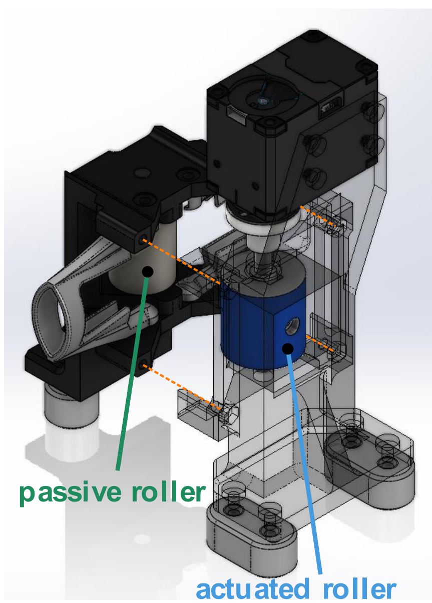

Figure 3.2: Extruder.

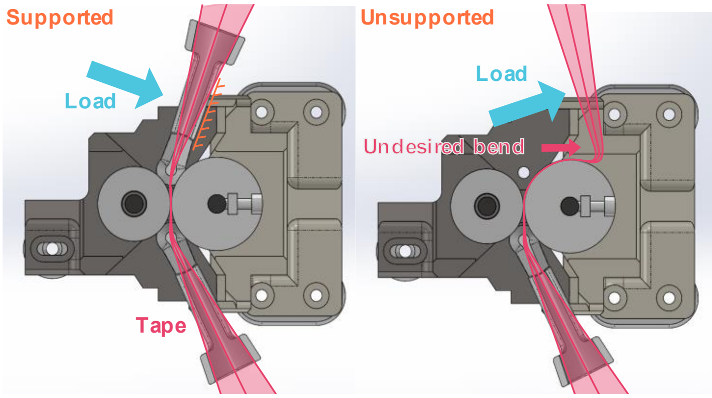

Figure 3.3: Guide.

3.1.3 Width control

Shown as Figure 3.4, linear motion of the rack and pinion mechanism is constrained by two 8mm diameter metal rods that serves as the guiding track. The pinion with the radius of 14mm is driven by a DYNAMIXEL XL430-W250-T motor mounted below the base. Supported by 3 linear bearings each extruder on the track can travel on the linear track smoothly. Notably, the center of extruders (the contact point of rollers) is symmetrically placed around the pinion's rotational axis, meaning a line defined by two centers of extruder does travel though the rotational axis but is not in parallel with the rack (i.e., the parameter *b* is different for the two sets of appendages) to decrease the minimum gap between the extruders and enlarge the range of size of objects that GRIP-tape can handle. For the same reason, the triangular shape is adopted in designing the extruders on the racks.

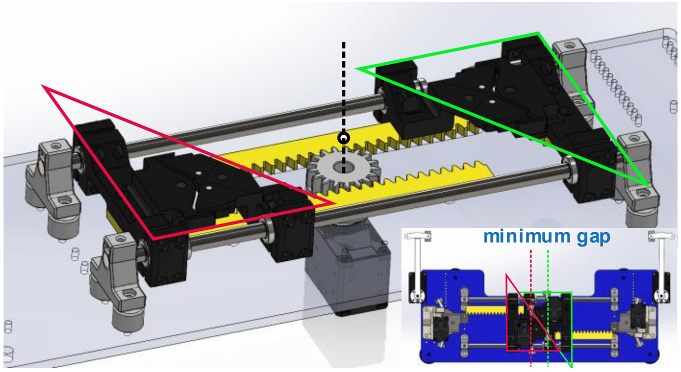

Figure 3.4: Rack and pinion.

3.1.4 Angle control

The angular control unit (Figure 3.5) is responsible for adjusting θ_4. On the tip of it installs guiding ring that help holding the tape. The rotation axis of the guiding ring is intentionally off set from the beam to decrease potential collisions between the beam and the tape during movement of the beam. Additionally, an 'x' shaped structure is integrated to stabilize the orientation of guiding ring, ensuring the tape's upright position and further enhancing the overall gripping performance.

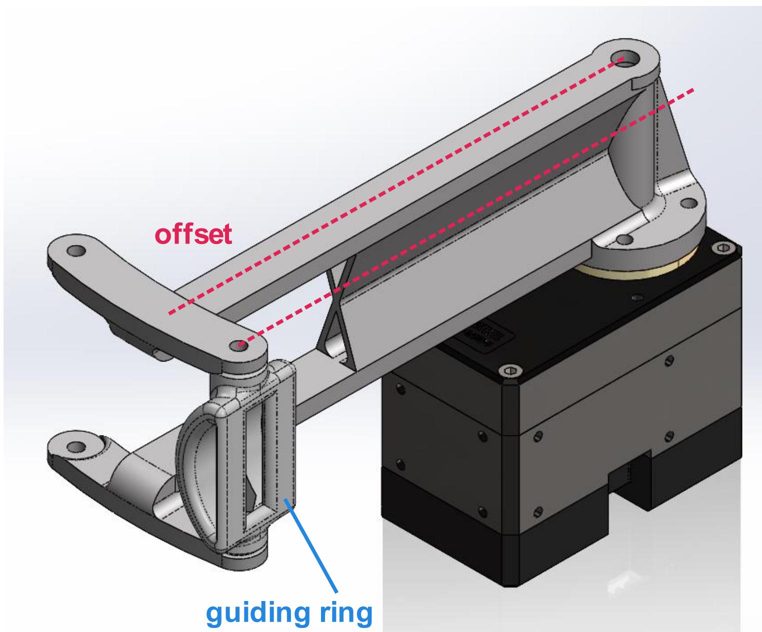

Figure 3.5: Angular control unit.

3.2 Programming

The control of GRIP-tape primarily relies on MATLAB, following the DYNAMIXEL Protocol 2.0. This protocol enables the assignment of goal positions and velocities to specific addresses, facilitating the manipulation of the gripper's movement. Additionally, it allows for the report of present positions, aiding in determining the current configuration of the appendages through forward kinematics.

3.2.1 Basic functions of single appendage

GRIP-tape is actuated by 7 DYNAMIXEL motors in extended position mode. Desired position can be reached with code provided by the manufacturer with assigning of position and velocity. Due to the built-in PID controller of DYNAMIXEL motors, no extra controlling of the position of motors is required.

Appendage transformation: Assuming the width control parameter a is known, the transformation of moving the center of the arc on the tip of the appendage to target location (x^*, y^*) was conducted by steps:

Step0: Set θ_{4i} to be 0, measure and input the initial L_{1i}, L_{2i}, L_{0i}. Record the states of both extruders and mark it as the initial state E_{1i} and E_{2i}.

Step1: Input the target coordinate (x^*, y^*) of the center of the tip of the appendage and solve the inverse kinematics with known parameter a to find new target L_1^*, L_2^*, L^* and θ_4^*.

Step2: Read the current state E_1 and E_2, current $L = L_i + (E_1 - E_{1i}) + (E_2 - E_{2i})$ and θ_4. The configuration of the appendage including the current length of L_1, L_2 can be derived.

Step3: ***Tip remain mode***: This mode ensures the object remains at a consistent relative distance in relation to the tip, particularly advantageous when the contacting point on the tape is close to the tip (refer to Figure 3.6). Throughout the transformation, both extruders function independently, each extending by the lengths of

$$\delta E_1 = \delta L - \delta E_2 = (L^* - L) - \delta E_2$$

and

$$\delta E_2 = \delta L_2 = L_2^* - L_2$$

As the inner surface (known as L_2) is the primary contact surface for the objects, in this mode what we want to ensure is $\delta E_2 = \delta L_2$ to make the point of tangency between link L_2 and arc L_3 on the physical tape keeps to be the point of tangency. Since the length of the curve L_3

varies during the transformation of the appendage, to make up the influence of δL_3, the computation of δE_1 relies on δE_2 and the difference between the target and current overall length δL.

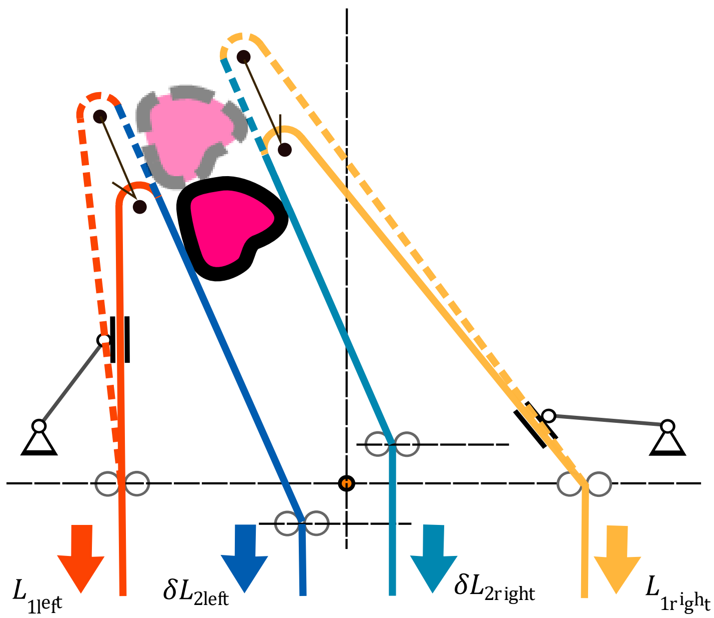

Figure 3.6: Tip remain mode.

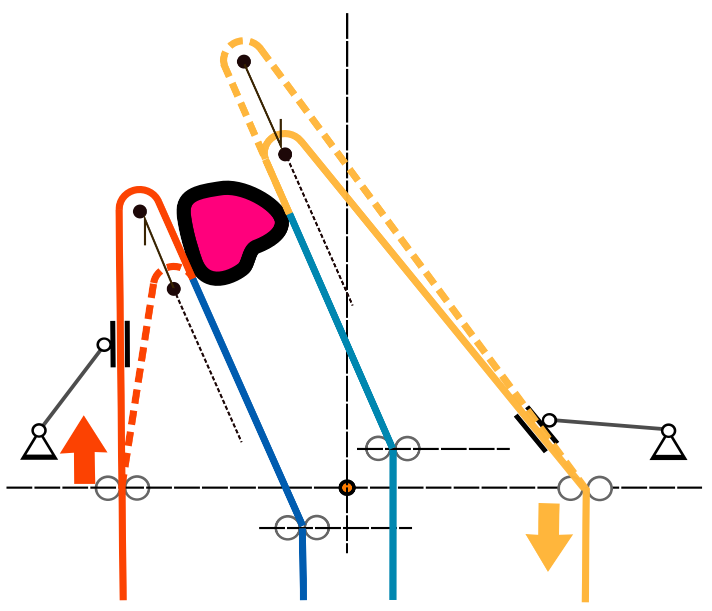

Figure 3.7: Outer only mode.

Outer only mode: In this mode, the transformation is conducted with only functioning the extruder that directly controls the otter half of the appendage. It allows the appendages adjusting their length while keeping an object in grip stays in the global coordinate. Since the contacting surface is stalled, the axial movement is prohibited, to fulfill the task, the assigned coordinate must land on a certain line parallel to L_2 to avoid movements of the object in the angular direction. (Figure 3.7)

Inner only mode: converse to the outer only mode, the inner only mode only drives the extruders that's on the track.

DYNAMIXELS stop after reaching the target positions controlled by the in-built PID controller.

Step4: If new location is assigned, return to step1

Rotation of appendage: Rotation of tape is conducted by extruding and retracting on 2 sides at the same speed. i.e., $\delta E_1 = -\delta E_2$. Since the overall length L ,angle θ_4, and width control parameter a is not changing, the shape of the appendage also keeps the same.

3.2.2 Basic functions of GRIP-tape

Combing 2 appendages and a rack-pinion mechanism controlling a, GRIP-tape can accomplish tasks like object gripping, translation, rotating, and conveying.

Gripping: By inputting the coordinate $X_{obj} = (x, y)$ and the size of the object, in order to make the inner section of the appendages in parallel when gripping the object, so that the gripping force counter each other to decrease the chance of slipping. The program adjusts the distance between the center of two inner extruders to d'(Figure 3.8) using the rack and pinion mechanism.

$$d' = w/\sin(\theta_{base}) - 2 * b/\tan(\theta_{base})$$

$$\theta_{base} = \tan^{-1}(|\, y/x\,|)$$

With the parameter a decided, assign coordinates

$$X_L = (x - (w/2 + r) * \sin(\theta_{base}), y + (w/2 + r) * \cos(\theta_{base}))$$

and

$$X_R = (x + (w/2 + r) * \sin(\theta_{base}), y - (w/2 + r) * \cos(\theta_{base}))$$

respectively to the left and the right appendage. To increase the gripping force, points with lower gap on the green axis that travel through both contact points can be assigned.

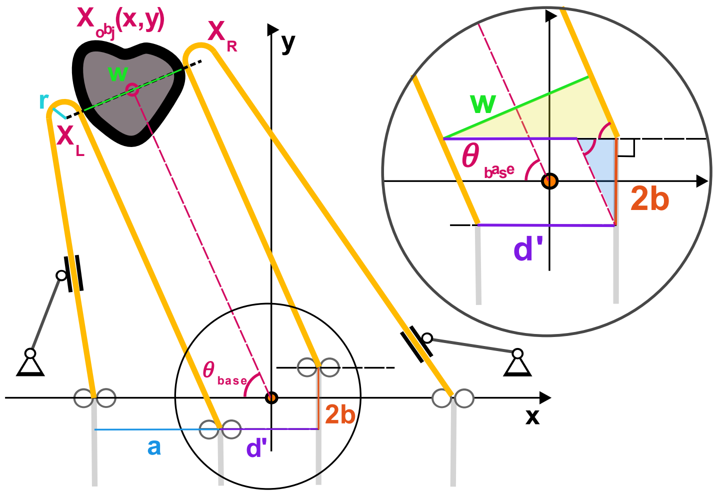

Figure 3.8: Width adjustment.

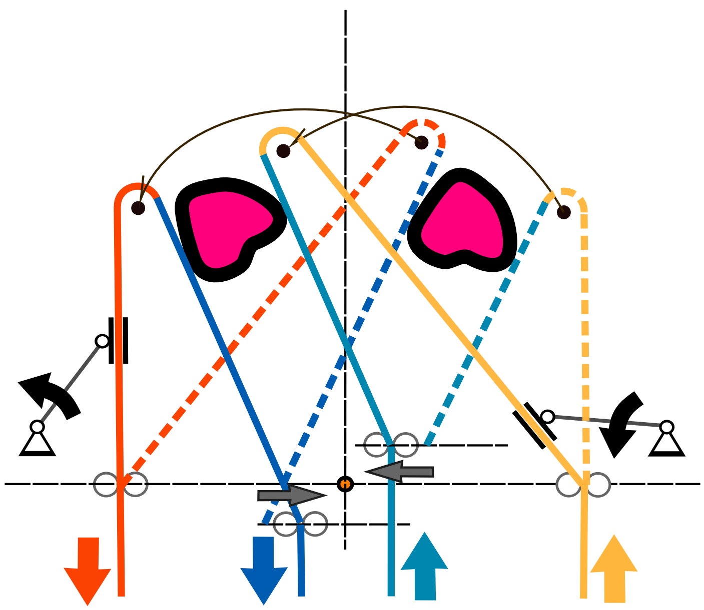

Figure 3.9: Object translation.

Translation: The translation of objects involves both gripping and appendage transformation, as depicted in Figure 3.9. Typically, it engages all 7 DYNAMIXEL motors. Upon receiving the object's target location, the program computes 2 sets of waypoints, each for one of the appendages along the trajectory from the current location to the target location, employing a similar approach described in the gripping process. Throughout the translation, the width is continuously adjusted to sustain the parallel configuration. During translation, a notable issue arises when assigning a constant velocity to all DYNAMIXEL motors between waypoints. This method does not result in a linear forward kinematics, meaning (x, y) don’t have linear relationship with any input, causing the actual trajectory of the arc's center to deviate from a straight line. Consequently, when holding an object, inconsistencies in the gripping force occur during translation, potentially leading mid-way drops. Presently, the solution involves setting closer waypoints to create a locally linear trajectory, aiming to mitigate this issue.

Rotation and conveying: These functions exclusively involve rotating the appendages. Object rotation occurs when both appendages rotate in the same direction and at equal speeds, causing the inner sections to move in opposing directions. The resulting friction forces counterbalance each other, yielding solely a rotational moment on the object, thereby initiating its rotation. Conveying, on the other hand, arises when the appendages rotate in opposite directions. It's crucial to highlight that conveying is feasible only when the gap between the inner sections of the appendages remains unchanged, i.e., the parallel alignment. Furthermore, within this setup, the rotational and conveying actions can be mixed by applying different rotation speeds to each appendage. For instance, by halting the rotation of one appendage, it works solely as a supportive track, enabling the object to roll in a specific direction on it.

3.2.2 App design

Utilizing MATLAB functions, an app was created using the MATLAB app designer (Figure 3.10). The app includes two switches for starting up the gripper. One is responsible for loading the library into MATLAB, while the other activates the motor power. Usually, before each operation, pressing the 'set initial' button reads the current positions of most motors and sets them as the initial states. For the angular control units, this button also drives the angular control links to desired initial angles. The 'to initial' button will drive the appendages back to their initial state within a given amount of time.

After the main switch turns on, the value of the x slider and the y slider will be assigned as the target location, and the two appendages will start to translate to this position the way discussed in section 3.2.2 with a mode chosen in the ‘Mode’ block. A while loop will keep checking the target location, and reading the current states of each motor. By changing the x and y values on the sliders, it will assign new target location to the appendages. Slider ‘w’ and ‘g’ are responsible for adjusting the gap between the two appendages at the base and the gripping force. The plot on the upper right will keep updating with the predicted lay out of the appendages after each input of a different target location. The ‘STOP’ switch is an emergency stop that stops any ongoing task when it is on.

The 'Auto' switch initiates the automatic object detection, measurement, and gripping process. 'F base', 'F tip', and 'F obj' display the force readings at the base, the predicted force at the appendages' tip, and the anticipated force on the object. Further explanation on these functions will be provided in Chapter 5.

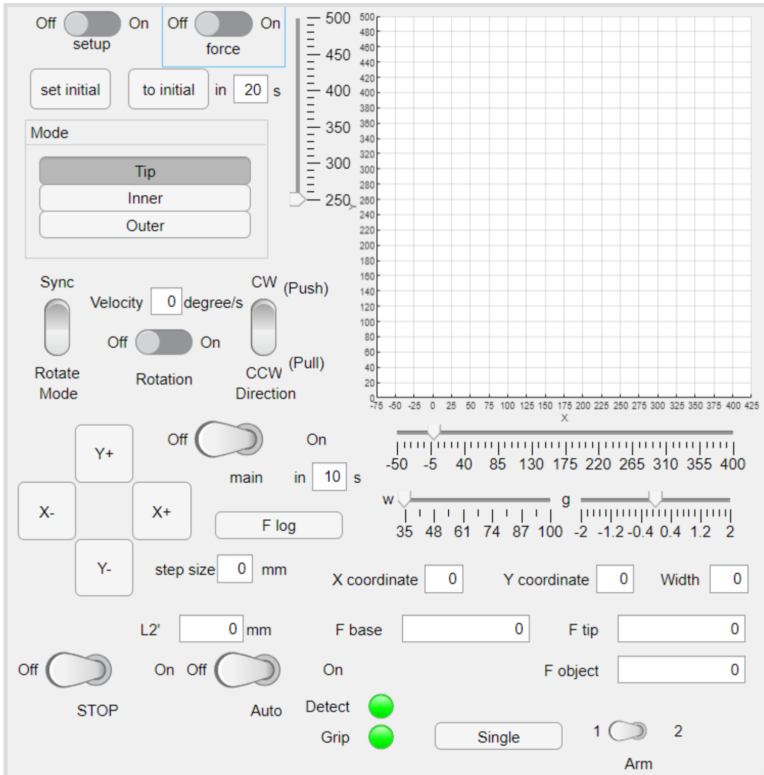

Figure 3.10: App design

3.2.3 Control with gamepad

The integration of gamepad control within the app enables object manipulation in location via Logitech F310's right joystick, adjusting the target location within a maximum of 10mm increment per loop cycle. The left joystick's x-axis regulates the 'w' parameter (gap), while the triggers (RT tighten & LT loosen) manage the 'g' (gripping force). Appendage rotation is linked to the shoulders (RB & LB) for different directions. Pressing either shoulder initiates object rotation, while button 'A' reverses the rotation direction of one appendage, conveying the object inward or outward based when the respective shoulder is pressed.

4.1 Validation

4.1.1 Gripping

By combining the data from the buckling force experiment and the workspace analysis, I generated a heat map illustrating the gripping force that GRIP-tape can sustain at different positions (refer to Figure 4.1). The calculation the maximum gripping force involves the relationship between the maximum torque resisting bending and the length of the supporting side of the appendage (i.e. the side connects to the angular control beam). For each point on the heat map, I use the Inverse kinematics to calculate the length of L_1 and the location of the sleeve P_4 on the angular control beam L_4. the supporting length is the upper section of the separated L_1 by P_4. Since for any objects on the 2D plane, the most supportive gripping gesture is using the tip pf the appendage to interact with the object, in the calculation of maximum gripping force, we are assuming the external force is applied on the tip of the appendage. This heat map reveals that GRIP-tape can handle the highest forces near the base, particularly in the central region. However, as the distance from the base increases and location laterally away from the central line (i.e. x = 175), the applicable gripping force diminishes.

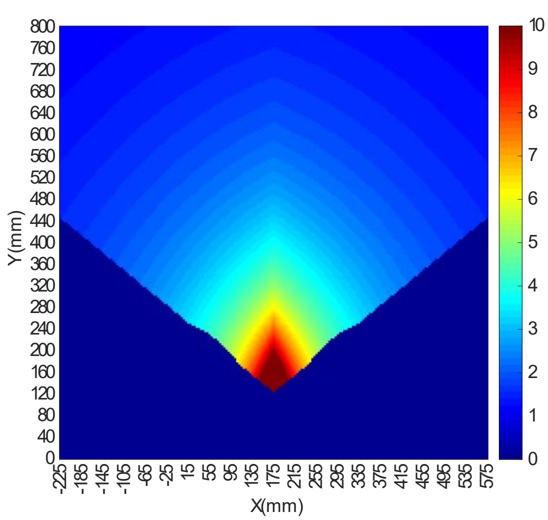

Figure 4.1: Heatmap of the max gripping force.

4.1.2 Extension

To find out how far an appendage can possibly reach, we designed a test that only involves the length control of one appendage of GRIP-tape without any perturbation. on both unidirectional and bidirectional tape springs. Due to gravity, oscillation, imperfections in fabrication, and the anisotropy of the unidirectional tape, one half of the appendage flips drastically and lose support in halfway while extending, this flip results in the failure of the appendage. The longest distance it reached was about 3.5ft. For the bidirectional tape, flipping is no longer a problem compared to the unidirectional tapes due to the bound of the duct tape and the support of the additional piece of tape spring. The longest distance we tried was about 5 ft without falling or buckling, different from the unidirectional tape, the limitation is mostly due to the extra gravity of electric tapes and duct tapes used to hold two pieces of tape spring together. Is hard to keep the appendages parallel to the floor with 3D-printed plastic parts and acrylic boards. A loaded example that highlights the stability is shown below as Figure 4.2. The appendage is tilted inward but still possess the supporting ability.

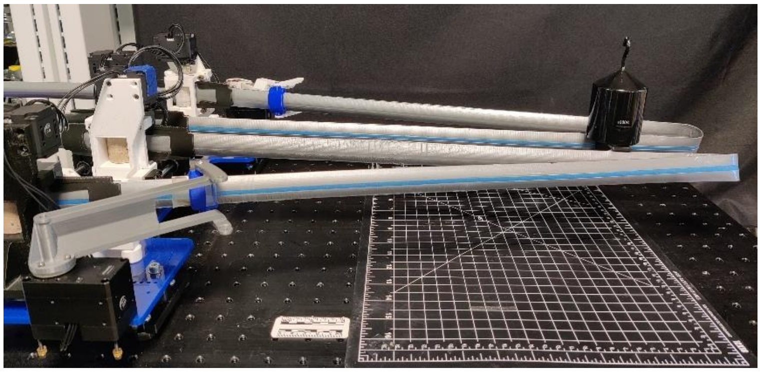

Figure 4.2: Stability of bidirectional tape resisting flipping

Although bidirectional has longer range of extension, spooling of it was not as easy as unidirectional tapes like regular tape measures. In the application of tape springs as tape measures, it is common to wind the tapes onto a spool, incorporating a pre-loaded spiral torsion spring and enclosing them within a cage. However, when it comes to bidirectional tapes, challenges arise due to variations in radius when its winded and the limitation on sliding posed by duct tape, causing asynchronization during the winding process. A solution to this issue will be explored in section 6.1.

4.1.3 Deformation

The softness of the appendage's tip opens up various possibilities for the gripper. Passively, encountering an obstacle along its intended path might result in the appendage deforming temporarily to navigate around it before reforming its triangular shape towards the intended endpoint (Figure 4.3a). This characteristic expands the gripper's fault tolerance in trajectory planning and ensures safer interactions upon contact.

With known obstacles and effective modeling, the deformed appendage remains functional, as depicted in Figure 4.3b, showcasing an application of this deformable configuration. The soft-rigid nature of tape appendages enables them to adapt to the environment while retaining the ability to withstand applied forces.

Assuming familiarity with the environment, there's potential to design an adaptive appendage capable of filling a confined 2D space, pressing against a target object, and conveying it out using the appendage's conveyor belt mode. Moreover, leveraging the adaptive deformation of the appendage, integrating sensors along the tapes might enable the creation of a physical environment scanner.

These potentials demonstrate the versatility and adaptability of the gripper's appendage, suggesting various applications in manipulation, environment interaction, and even potential sensory capabilities, expanding its utility in diverse scenarios.

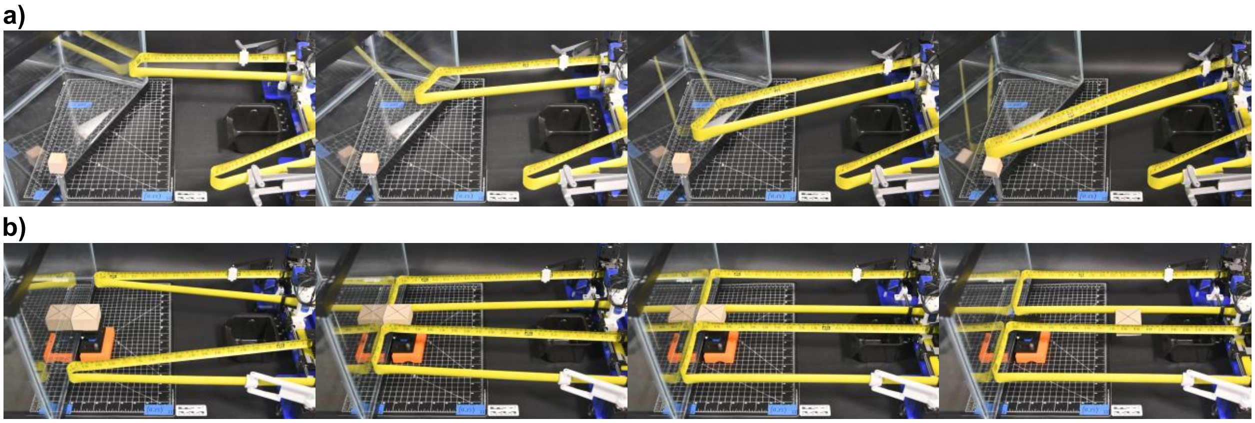

Figure 4.3: Demonstrations of deformation.

4.2 Demonstrating basic capabilities of GRIP-tape

4.2.1 Translation

For each appendage of GRIP-tape, there are two tape extruders that are designed for extending and retracting the tape spring. the extruder consists of a frame and two rollers, one of the rollers is connected to a motor and transfers the rotation to the translation of the tape spring. With the application of inverse kinematics, by inputting x and y, we are able to point the tip at any coordinate in the reachable range under the limit of the structure.

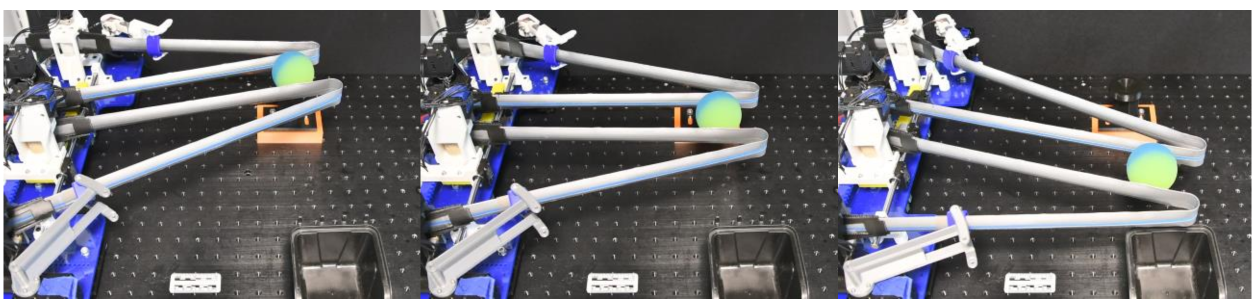

Figure 4.4: In-hand translation

4.2.2 Gripping

One specific feature of the tape spring is anisotropy. The tape spring can be seen as a rigid beam if the force is applied to the convex face, however, the concave face can hardly supply any force. The idea of making a tape spring become an appendage is by creating a buckling at the tip and bending the tape spring so that the convex face is pointing outward on both sides of the appendage. In this way, the appendage is rigid on both sides. During gripping, the buckling section is transferring the force from the outer section to the inner section. The amount of force is visible and is reflected by the curvature of the buckling section in a positive correlation (Figrue4.5).

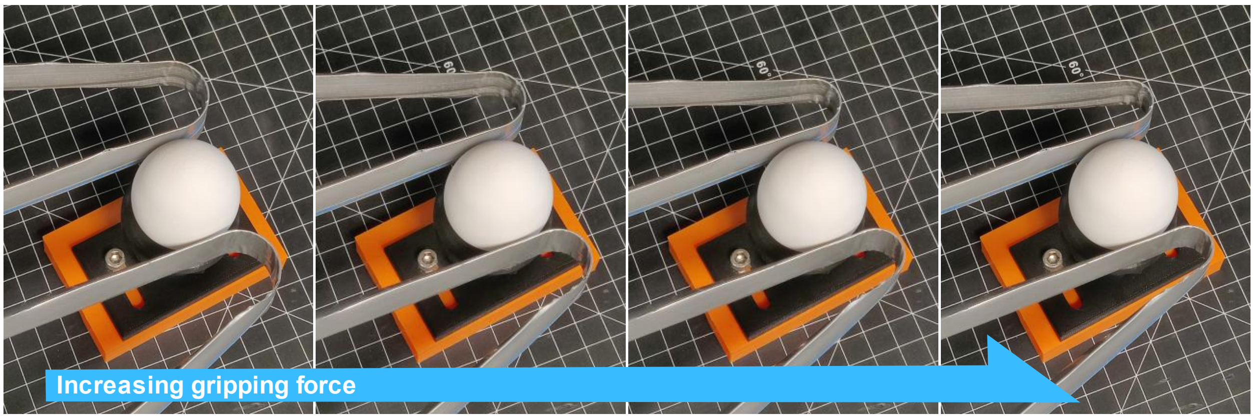

Figure 4.5: Gripping.

4.2.3 In-hand manipulation

Once both the two appendages of GRIP-tape contact with the targeting object, we can change its orientation by moving the inner section of both appendages in opposite directions. In the meantime, to keep the overall lengths of both appendage constant, the tape extruders for each appendage should also operate accordingly. For example, if we want to rotate a ball of a radius of r by 90 degrees. the surface on the inner section of the tape of the left appendage has to extend $r * \pi/2$. To make the ball stay at a constant location, the inner section of the tape of the right appendage has to retrieve $r * \pi/2$. Accordingly, the outer section of the left appendage retrieves $r * \pi/2$, and the outer section of the right appendage extends $r * \pi/2$. Another application of it utilizes the surface of tape springs as conveyor belts to pull and firmly grip the object in a sequence.

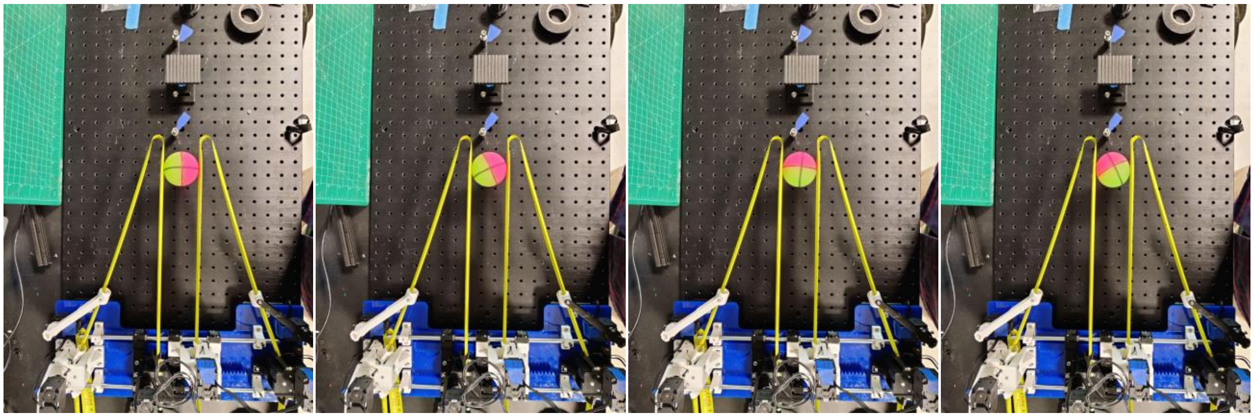

Figure 4.6: In-hand rotation

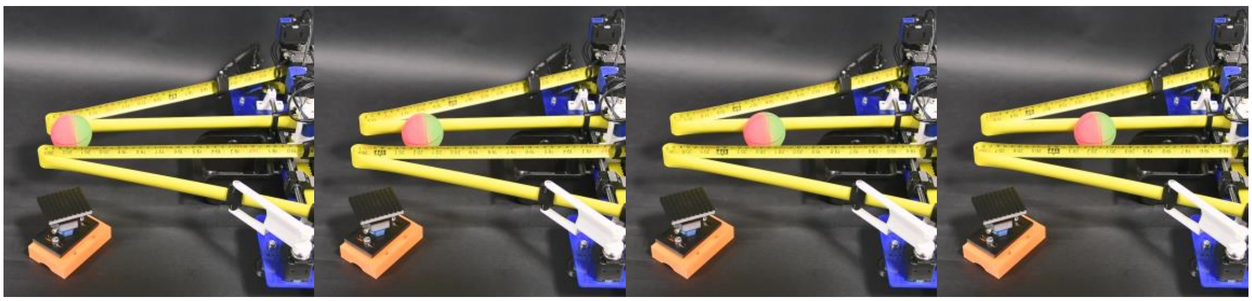

Figure 4.7: Conveying.

4.3 Applications

In Figure 4.8, real-life applications of GRIP-tape showcasing its fundamental capabilities are illustrated. In Figure 4.8a, GRIP-tape exhibits its ability to maneuver a bouncy ball using both inverse kinematics and conveying methods. Figure 4.8b highlights the gripper's adeptness in handling delicate objects by delicately pinching a tomato and removing it from its vine with a twisting motion. In Figure 4.8c, GRIP-tape demonstrates its capacity to vertically transport an object, counteracting gravity, as depicted by handling a fresh lemon.

Moreover, attempts were made to utilize GRIP-tape's capabilities in tasks such as transferring and inserting a bulb into a socket, twisting it to illuminate, as well as using the gripper appendages to secure and bolt in a fastener using a screwdriver.

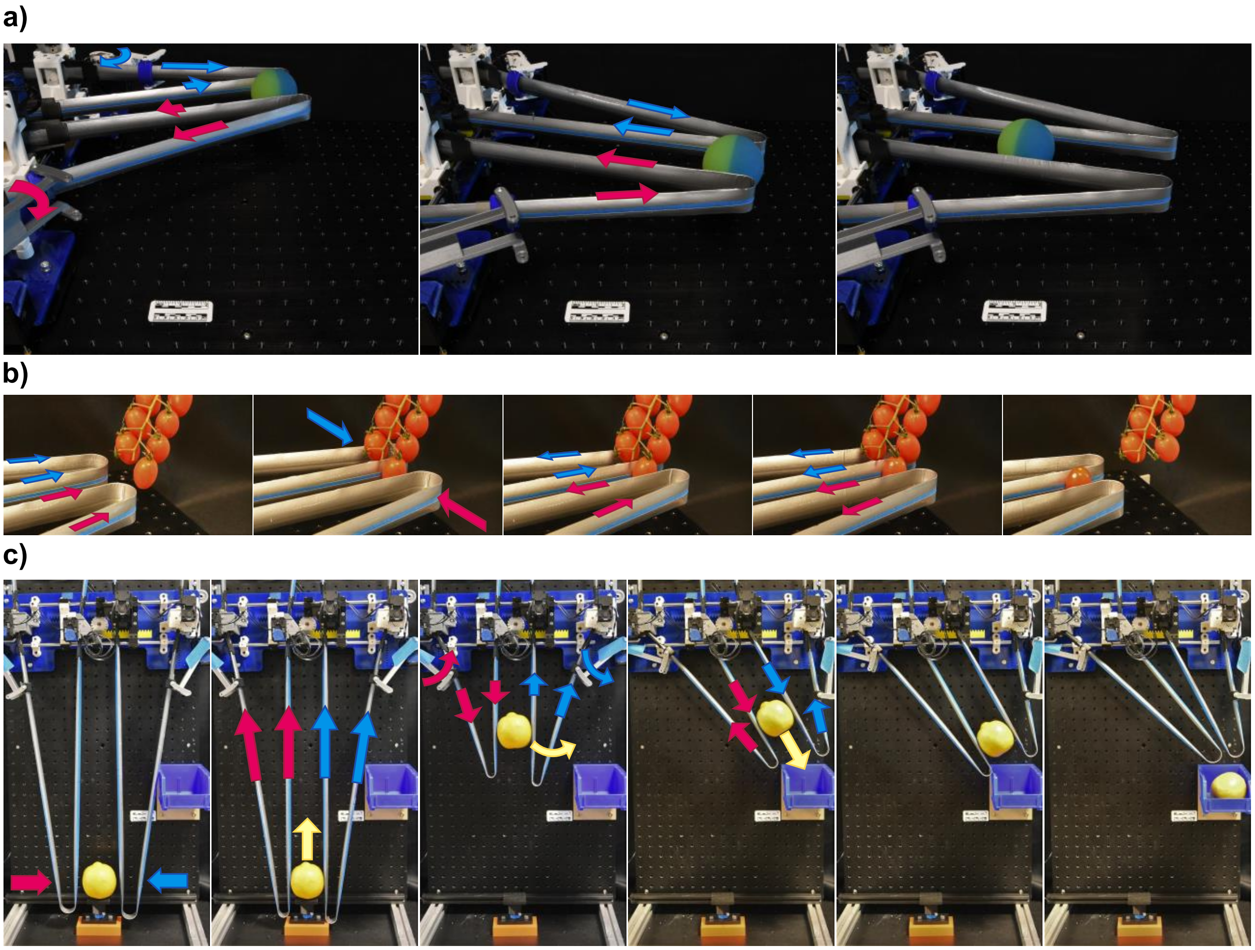

Figure 4.8: Demonstrations

Chapter 5 GRIP-tape: advanced applications

5.1 Force sensing

Adding a load cell on the angular control beam helps us with sensing the gripping force (Figure 5.1). If the moment on the appendage is balanced, with knowing θ_4 and L we can derive θ_1, θ_2, L_1 and L_2' by forward kinematics. With balancing the moments, the relationship between the force on the inner section and the read of the load cell is:

$$F_1' = F_{read}/cos(\theta_1 - \theta_4)$$

$$F_1 = (F_1' * L_1' + \tau_1)/L_1$$

$$F_2 = F_1$$

$$F_2' = (F_2 * L_2 + \tau_2)/L_2'$$

F_{read} is the reading of the load cell, and τ_1 and τ_2 represent the resilience of the bent tape spring.

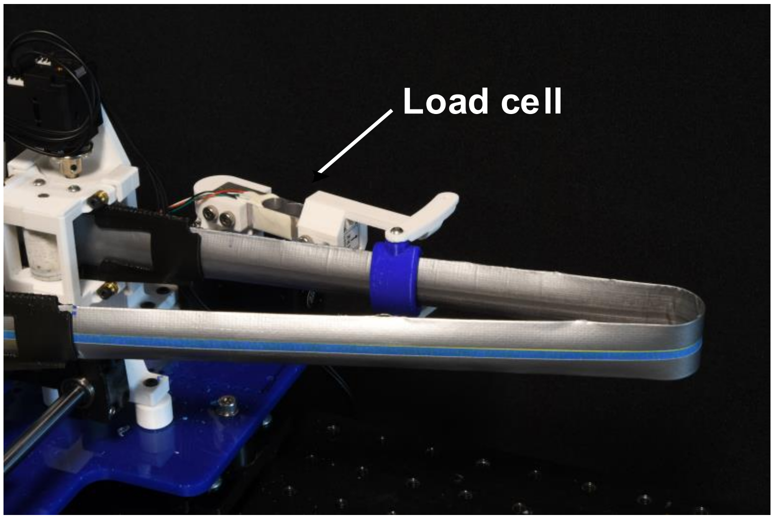

Figure 5.1: Load cell on the angular control unit.

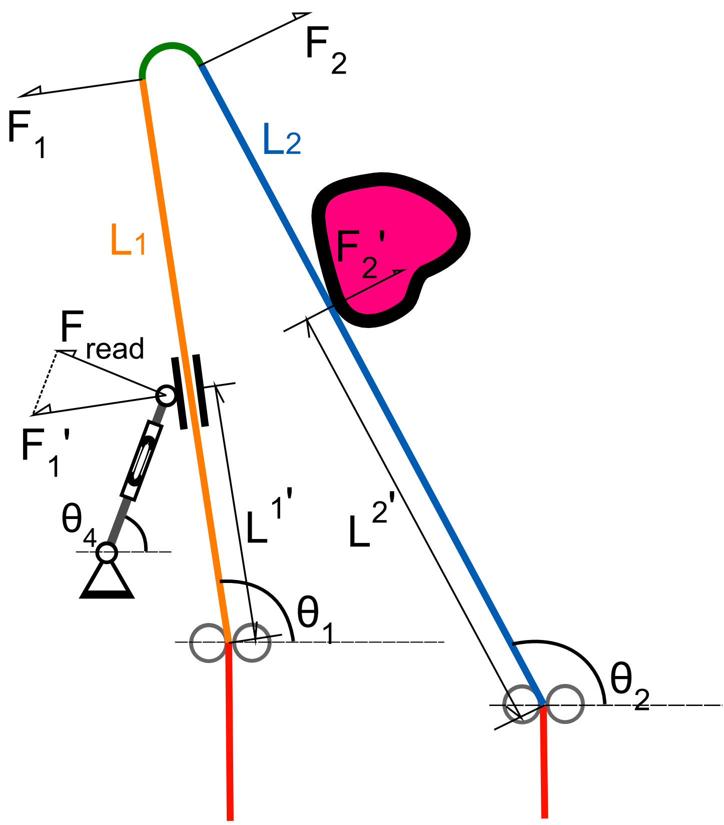

Figure 5.2: Balance of moment.

To obtain τ_1 and τ_2 at different angles, I conducted measurements on the recovery moment of a bi-directional tape that was bent around a pinched point. This involved bending it to multiple angles and recording the resulting moments. Employing spline curve-fitting on this data revealed a correlation between the bending angle and τ. To validate the force sensing, I installed another load cell at the appendage's tip for comparison. Figure 5.4 illustrates a comparison between the actual force at the appendage tip and the computed value F_2 derived from the base's force reading F_{read}. This comparison demonstrates that the maximum error remained below 0.2N, meeting our application requirements for gripping.

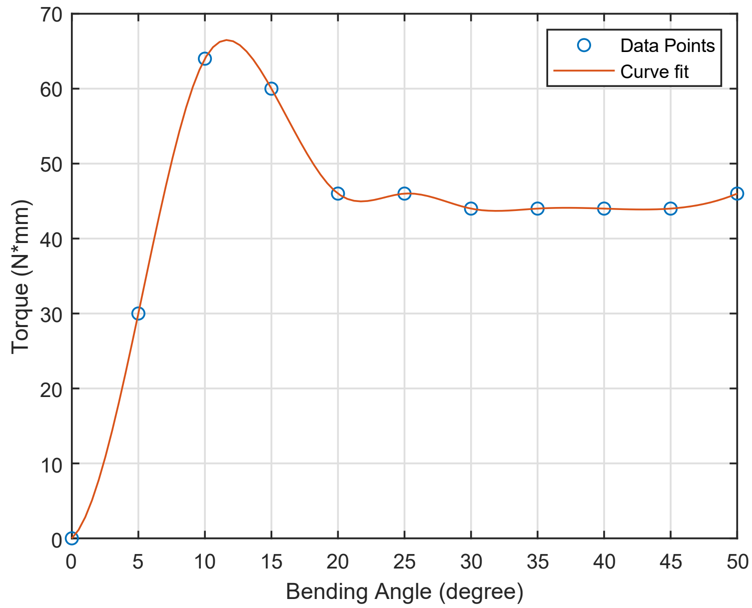

Figure 5.3: recovering moment of bent bidirectional tape.

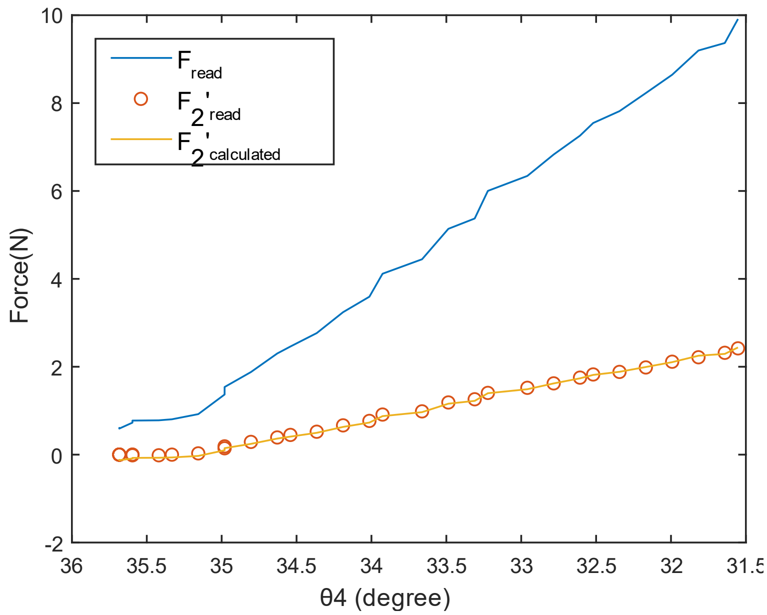

Figure 5.4: Comparison of forces

5.2 Automatic gripping

I designed several motion steps to complete automatic gripping (Figure. 5.5). Step 1 and step 2 are designed for searching and detecting the object with the tip of the left appendage and the right appendage traveling along a predefined curve centered at the origin. The sign of the ending of both steps is the increase of the predicted force F_2 at the tip of the appendage. After step 2, we can define a certain line where the object is located but are still unsure about the size of the object. For step 3 and step 4, GRIP-tape separate its appendages and close them in parallel. With another increase of F_2, which indicates the contact with the object, we can define the width of the object w. If controlling the gripping force is not required, then we don't need to move the object to the tip of the appendage, step 4 is the last step. With paralleled appendages, GRIP-tape can convey the object outward until it is pushed out and dropped into a target location as long as the location of the exit is determined. If there is a need to restrict gripping force on the object, to define the distance to the object i.e. the value of L_2', step 5 will be conducted. Retracting one of the appendages with only the outer extruder shortens the appendage while keeping the object remain the same place. The retraction stops when F_2 is below a certain threshold right before detachment, at the same time, with Forward kinematics we know the value of L_2'. The last step is moving the two appendages to the location of the object and closing them to make the gap between the appendages equal to the width of the object w. Then slowly increase the gripping force until the calculated F_2' reaches the desired value.

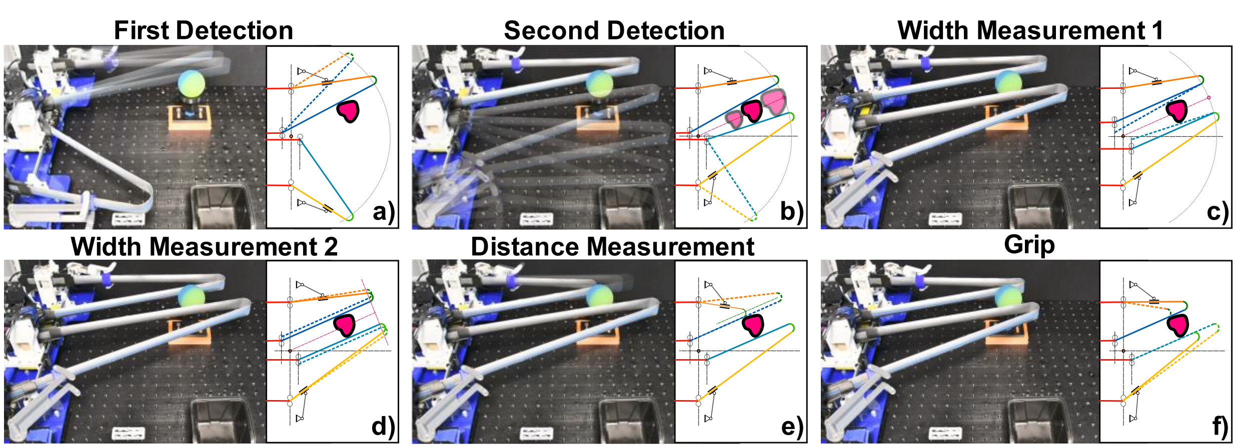

Figure 5.5: Demonstration of automatic gripping

Chapter 6 Accessories of GRIP-tape

6.1 Spool

In the application of tape springs as tape measures, it is common to wind the tapes onto a spool, incorporating a pre-loaded spiral torsion spring and enclosing them within a cage. However, when it comes to bidirectional tapes, challenges arise due to variations in radius when its winded and the limitation on sliding posed by duct tape, causing asynchronization during the winding process (Figure 6.1). To address this issue, our solution is binding two tapes with a sleeve made of low friction film, allowing them to slide internally. Based on the design of the spool of tape measures, we combined a case specifically designed for bidirectional tapes and a spool sourced from Amazon Basic tape measures, featuring an integrated spiral torque spring. A demonstration of spooling is shown as Figure 6.2.

Figure 6.1: Inner split of winded bidirectional tape

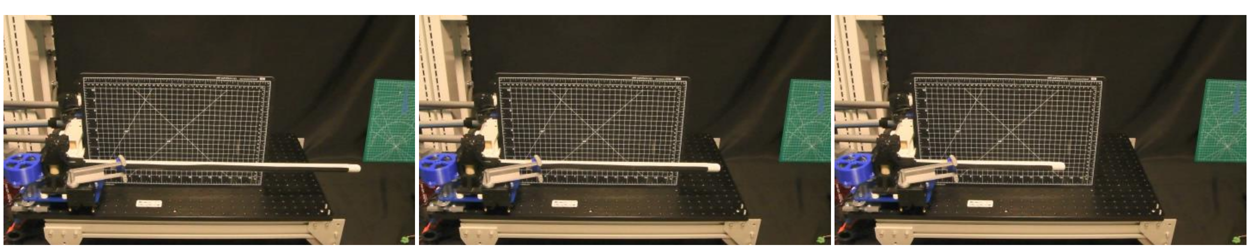

Figure 6.2: Spooling

6.2 Stiffing sleeve

As outlined in section 4.1.3 Deformation, the tip of the appendage exhibits susceptibility to deformation under external loads. Specifically, bidirectional tape starts to experience deformation when subjected to pressures approximately 5N when pressed against a surface.

To address this issue, especially when such flexibility is undesirable for specific tasks, I developed a sleeve designed to follow the appendage's tip, independent of the change in appendage's shape. This structure effectively maintains the shape of the tip when encountering external collisions. Consequently, the maximum resistance to pushing forces increased to over 50N, the stiffness limit is confined by the material and structure of the 3D printed PLA used for the stiffing sleeve, suggesting a potential enhancement through the adoption of metal components to strengthen durability and stiffness.

The sleeve's functionality is facilitated by six bearings positioned along its curved surface and a central roller, crucial elements that ensure fluent movement of the stiffening sleeve along the tapes. The wall of the sleeve works the same way as the guides on the extrudes preventing immersing undesired bends, enhancing its structural stiffness.

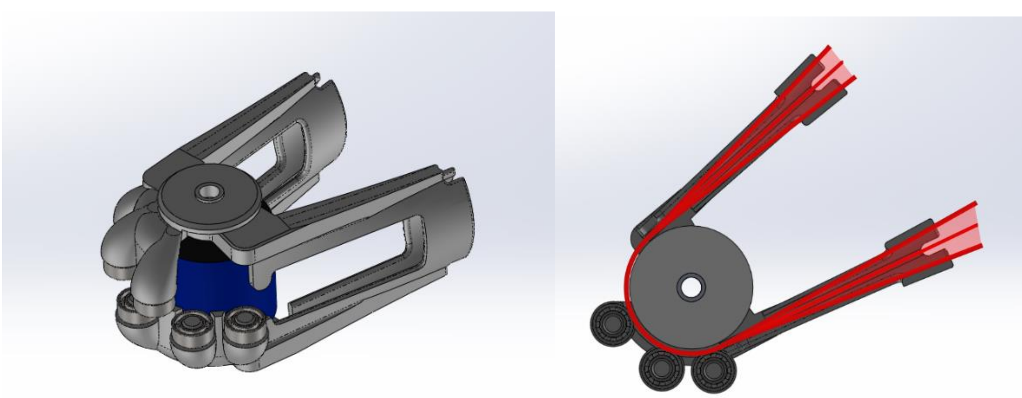

Figure 6.3: Stiffening Sleeve

CONCLUSION

In this thesis, an exploration of GRIP-tape, an innovative design merging tape springs with control mechanisms, has been presented. This research endeavors to address the multifaceted challenges in object searching, soft gripping, manipulation, and force sensing contributing to the burgeoning field of robotic grippers and manipulators.

The first two chapters introduced the fundamental concepts underlying GRIP-tape, elucidating its design, modeling, and kinematics. By testing and analyzing features of bidirectional tape, crucial insights were gained, forming the basis for GRIP-tape's functionality. A pair of inverse and forward kinematics models was created controlling the shape of appendages. With identifying necessary parameters, the design schematics of GRIP-tape was created.

The CAD design of GRIP-tape was crafted on SolidWorks and programming executed through MATLAB, featuring a user-friendly app. The logic of controlling the transformation of appendages was discussed including different transformation modes for the appendage. For gripping and translating, an adjustment of the gap in between the appendages was introduced.

In the following chapter, the practical applications of GRIP-tape's capabilities were explored and demonstrated. The validation process elucidated the gripping force mapping, revealing its strengths and limitations within the workspace. The feature of deformation on the appendages was also discussed. The functionality of soft gripping, translation, and rotation was effectively showcased through real-world objects such as tomatoes, and lemon, underscoring the versatile utility of GRIP-tape across diverse scenarios and objects.

Advanced applications expanded GRIP-tape's functionalities by integrating force sensing mechanisms and automatic gripping sequences. The incorporation of load cells for force detection and automatic gripping sequences offered promising avenues for autonomous and adaptive manipulation tasks.

The spool mechanism, along with an alternative fabrication approach for bidirectional tape, tackled the challenge of spooling. Additionally, the stiffening sleeve was introduced to counter undesired deformation, preserving structural integrity while executing various manipulation tasks. These accessories significantly contribute to enhancing GRIP-tape's versatility and operational efficiency.

The findings and innovations presented in this thesis lay a solid foundation for future research and advancements in robotic manipulation and gripper technologies. As the field progresses, leveraging the principles elucidated here can propel developments in versatile and adaptable robotic manipulation systems.

FUTURE STUDIES

Closed-loop control: Ensuring smooth object translation without undesired pauses at waypoints is pivotal. incorporating load cells mentioned in chapter 5 as sensors could pave the way for a closed-loop control system. This system would enable continuous adjustment of appendage positions, ensuring sustained gripping force throughout object translation.

Deformation and sensing: Exploring the appendages' deformable nature (as detailed in Section 4.1.3) reveals potential applications worth further investigation. These include leveraging active deformations for varied tasks and employing deformable appendages for efficient gripping by filling spaces with tape and a potential of environment learning using physical method with sensors along the tape.

Additional appendages: A critical limitation of GRIP-tape as a manipulator lies in its two counter placed appendages, confining its functionality to a 2D plane. Introducing an additional appendage and adopting a triangular layout could expand its manipulation capabilities, offering enhanced gripping performance with at least one supporting appendage beneath the object.

Variations in tape design: Exploring alternative tape configurations during GRIP-tape development presents avenues for improving gripping performance beyond relying solely on friction. For instance, a '8' tape configuration built from four pieces of tape could improve gripping performance while enabling extension and translation. Strengthening specific tape segments to enhance maximum gripping force, such as adding extra tape layers in areas prone to buckling, might be beneficial. This adjustment might necessitate corresponding changes in roller design, favoring flexible rollers that can accommodate varying tape thicknesses over rigid ones that struggle with such diversity.

REFERENCES

[1] A. Kakogawa, H. Nishimura, and S. Ma, “Underactuated modular finger with pull-in mechanism for a robotic gripper,” in 2016 IEEE International Conference on Robotics and Biomimetics (ROBIO), 2016, pp. 556–561.

[2] V. Tincani, M. G. Catalano, E. Farnioli, M. Garabini, G. Grioli, G. Fantoni, and A. Bicchi, “Velvet fingers: A dexterous gripper with active surfaces,” in 2012 IEEE/RSJ International Conference on Intelligent Robots and Systems, 2012, pp. 1257–1263.

[3] K. Morino, S. Kikuchi, S. Chikagawa, M. Izumi, and T. Watanabe, “Sheet-based gripper featuring passive pull-in functionality for bin picking and for picking up thin flexible objects,” IEEE Robotics and Automation Letters, vol. 5, no. 2, pp. 2007–2014, 2020.

[4] E. W. Hawkes, L. H. Blumenschein, J. D. Greer, and A. M. Okamura, “A soft robot that navigates its environment through growth,” Science Robotics, vol. 2, no. 8, p. eaan3028, 2017. [Online]. Available: https://www.science.org/doi/abs/10.1126/scirobotics.aan3028

[5] L. H. Blumenschein, L. T. Gan, J. A. Fan, A. M. Okamura, and E. W. Hawkes, “A tip-extending soft robot enables reconfigurable and deployable antennas,” IEEE Robotics and Automation Letters, vol. 3, no. 2, pp. 949–956, 2018.
18

[6] P. Li, Y. Zhang, G. Zhang, D. Zhou, and L. Li, “A bioinspired soft robot combining the growth adaptability of vine plants with a coordinated control system,” Research, vol. 2021, 2021. [Online]. Available: https://spj.science.org/doi/abs/10.34133/2021/9843859

[7] S.-J. Kim, D.-Y. Lee, G.-P. Jung, and K.-J. Cho, “An origami-inspired, self-locking robotic arm that can be folded flat,” Science Robotics, vol. 3, no. 16, p. eaar2915, 2018. [Online]. Available: https://www.science.org/doi/abs/10.1126/scirobotics.aar2915

[8] S. Wu, Q. Ze, J. Dai, N. Udipi, G. H. Paulino, and R. Zhao, “Stretchable origami robotic arm with omnidirectional bending and twisting,” Proceedings of the National Academy of Sciences, vol. 118, no. 36, p. e2110023118, 2021. [Online]. Available: https://www.pnas.org/doi/abs/10.1073/pnas.2110023118

[9] J. Tanaka and N. Matsuhira, “Development of a parallel gripper with an extension nail mechanism using a metal belt,” MM Science Journal, vol. 2021, no. 2, p. 4444–4451, 2021.

[10] Y. Yang, Y. Qin, Y. Tang, Y. Yang, Y. Peng, and H. Pu, “Deployable closed-loop tape-spring manipulators with mobile drive components on localized folds,” Mechanism and Machine Theory, vol. 167, p. 104553, 2022. [Online]. Available: https://www.sciencedirect.com/science/article/pii/S0094114X21003001

[11] J. Quan and D. Hong, “Extending and bending robotic limbs using tape springs for mobility

and manipulation: Preliminary investigations,” vol. Volume 7: 46th Mechanisms and Robotics Conference (MR), 2022, p. V007T07A044.

[12] C. Sparks, N. Justus, R. Hatton, and N. Gravish, “Amoeba-inspired swimming through isoperimetric modulation of body shape,” in 2022 IEEE/RSJ International Conference on Intelligent Robots and Systems (IROS), 2022, pp. 2685–2692.

[13] C. Sparks, and N. Gravish, "Pressure control of rolling-seal tape spring actuators", 2024 IEEE International Conference on Soft Robotics, under review.

[14] D. Rus and M. Tolley, “Design, fabrication and control of soft robots,” Nature, vol. 521, pp. 467–75, 05 2015.